

# CHALMERS



## Boiling in liquid hydrogen under gravity compensated with a magnetic field

Measure of the thermal heat transfers in liquid hydrogen in nucleate and film boiling regime under gravity compensated with a magnetic field

*Master of Science Thesis in the Master's Programme Applied Physics*

STEPHANE GARCIA

Department of Applied Physics  
CHALMERS UNIVERSITY OF TECHNOLOGY  
Göteborg, Sweden 2012  
Master's Thesis 2012





Master of Science Thesis 2012

# Boiling in liquid hydrogen under gravity compensated with a magnetic field

Measure of the thermal heat transfers in liquid hydrogen in nucleate and film boiling regime under gravity compensated with a magnetic field

STEPHANE GARCIA

Department of Applied Physics  
CHALMERS UNIVERSITY OF TECHNOLOGY  
Göteborg, Sweden 2012

Boiling in liquid hydrogen under gravity compensated with a magnetic field  
Measure of the thermal heat transfers in liquid hydrogen in nucleate and film boiling  
regime under gravity compensated with a magnetic field

©STEPHANE GARCIA, 2012

Master of Science Thesis  
Department of Applied Physics  
Chalmers University of Technology  
SE-412 96 Göteborg  
Sweden

Telephone + 46 (0)31-772 1000

Cover: A rocket taking off for space

Reproservice, Chalmers University of Technology,  
Sweden 2012

## Acknowledgements

First I want to thank Mr. Alain GIRARD, head of the Low Temperature Laboratory at CEA Grenoble and Mr. François VIARGUES, head of the Cryogenics for Fusion Group for having welcomed me.

Foremost I want to thank my advisor Denis Chatain. It has been an honour to work with him. He has taught me, both consciously and unconsciously, how good experimental physics is done. I appreciate all his contributions of time, ideas, and funding to make my Master's degree's experience productive and stimulating. The enthusiasm he has for his research was contagious and motivational for me. I am also thankful for the excellent example he has provided as a successful engineer.

I also thank Mr Janusz Kansky, my supervising teacher in Sweden for his advices about the writing of this master thesis report.

I really appreciated the advices of Pr. Jerome DUPLAT. His knowledge on heat transfer and boiling were very useful.

The support and supervising of Mr. Denis HITZ were very appreciated. I would like to acknowledge honorary Mr. François DEBRAY for the supervising of the magnetic part of the experiment and Mr. Christophe TROPHIME for his help during the calculation of the magnetic maps.

The support team of CEA, especially Jerome CHARTIER, Jean-Marc MATHONNET and Patrick BONNAY and the support team of LNCMI: Robert, Claude, Cedric and Romain who have contributed immensely to my professional time at Grenoble, and I would like to thank them a lot for that. This group has been a source of good advices and collaboration.

# Abstract

Nowadays, the behaviour of fluids in weightlessness is a great interest for a lot of scientists all around the world. A particular aim of this study is to predict how fluids behave in space. The use of cryogenic propellant - liquid hydrogen ( $LH_2$ ) and liquid oxygen ( $LO_2$ ) - is increasing, especially in space launcher. The main questions the designers of these launchers have to solve is how heat transfer are taking place in absence of gravity and how does the gravity affect the boiling crisis.

Experiments have been performed at the Low Temperature Laboratory (SBT) of the CEA/GRENOBLE in 2009 to answer this question for liquid oxygen. The experiments that are carried out in this master thesis are based on the same principle. However, the studied fluid is  $LH_2$ . It consists on measuring the thermal transfers in nucleate and film boiling regime for different levels of gravity, until 0g. The compensation of gravity is done by using a huge magnetic field, leading to an important gradient of this field, used to levitate the hydrogen. Such a facility is available at the CNRS of Grenoble in the National Laboratory of the Intense Magnetic Fields (LNCMI). This resistive coil of 20MW delivers a magnetic field of 15 Teslas.

For various thermal heat flux, the temperature difference between the wall and the fluid has been measured to plot the boiling curve : Nukiyama curve. These experiments have been carried out for several level of gravity and thermodynamics conditions (pressure and temperatures have been studied independently).

Results were very satisfying and the main goal of this study has been achieved: these results are able to answer the main questions of designers for the new Vinci engine, used in the next generation of spacecraft Ariane.

# Contents

<b>1</b>	<b>Introduction</b>	<b>1</b>
1.1	Context . . . . .	1
1.2	The study . . . . .	1
<b>2</b>	<b>Background</b>	<b>2</b>
2.1	Classical techniques to obtain microgravity . . . . .	2
2.1.1	Drop tower . . . . .	2
2.1.2	Parabolic flights . . . . .	3
2.1.3	Space shuttle . . . . .	3
2.1.4	Space station . . . . .	3
2.1.5	Magnetic compensation . . . . .	4
2.2	Gravity compensated by a magnetic field . . . . .	5
2.2.1	Principle . . . . .	5
2.2.2	Inhomogeneity of the compensation field . . . . .	6
2.2.3	Magnetic compensation in a simple solenoid . . . . .	7
2.2.4	Vector analysis . . . . .	7
2.2.5	Axial stability . . . . .	8
2.2.6	Radial instability . . . . .	10
2.2.7	Modification of the gravity level . . . . .	10
2.3	Heat transfer in boiling fluids . . . . .	12
2.3.1	Three modes of heat transfer . . . . .	12
2.3.2	Boiling . . . . .	13
2.3.3	Nukiyama curve . . . . .	14
2.3.4	Nucleate boiling . . . . .	17
2.3.5	Critical Heat Flux . . . . .	18
2.4	Information about hydrogen . . . . .	20
<b>3</b>	<b>Methods and materials</b>	<b>21</b>
3.1	The experimental setup . . . . .	21
3.1.1	The cryostat . . . . .	22
3.1.2	The observation system . . . . .	25
3.1.3	The experimental cell . . . . .	27
3.1.4	Thermal sensors . . . . .	30
3.1.5	The magnetic map . . . . .	30
3.2	Sizing of some elements . . . . .	31
3.2.1	Sizing of the current supply wire . . . . .	32
3.2.2	Sizing of the thermal shield heat exchanger . . . . .	34
3.3	Experimental protocol . . . . .	36
3.3.1	Starting the installation . . . . .	37
3.3.2	Stopping the installation . . . . .	39
3.3.3	Running of a measurement campaign . . . . .	40

<b>4</b>	<b>Results</b>	<b>43</b>
4.1	At 1g . . . . .	44
4.1.1	1bar at saturation . . . . .	44
4.1.2	1bar and $T=T_{sat}-2K$ . . . . .	45
4.1.3	2 bars and $T = T_{sat}-0.5K$ . . . . .	46
4.1.4	2 bars and $T = T_{sat}-2K$ . . . . .	47
4.2	At 0g . . . . .	48
4.2.1	1 bar and $T=T_{sat}-2K$ . . . . .	48
4.2.2	2 bars and $T=T_{sat}-2K$ . . . . .	50
4.3	Under 0.1g . . . . .	51
4.3.1	2 bars and $T=T_{sat}-2K$ . . . . .	51
<b>5</b>	<b>Discussion</b>	<b>52</b>
5.1	Corrections . . . . .	52
5.1.1	Temperature of the heating part . . . . .	52
5.1.2	Pressure in the cell . . . . .	53
5.1.3	Power transfered to the liquid . . . . .	53
5.2	Uncertainties on the losses related to the titanium ring . . . . .	55
5.3	Comparisons . . . . .	56
5.3.1	Effect of the gravity . . . . .	56
5.3.2	Effect of the pressure . . . . .	57
5.3.3	Effect of the subcooling . . . . .	58
5.4	Problems encountered . . . . .	59
5.4.1	Leakage in the cell feeding circuit . . . . .	59
5.4.2	Fast breakdown of the magnetic field . . . . .	60
5.4.3	Losses in the cooling circuit . . . . .	61
<b>6</b>	<b>Conclusion</b>	<b>62</b>
	<b>Appendices</b>	<b>63</b>

# 1 Introduction

## 1.1 Context

Studies on fluid are of a great interest for many scientific teams. They enable to predict the behaviour of a fluid and then to size as precisely as possible each component of a system. The following study is focused on cryogenic fluids used in space launchers: liquid hydrogen ( $LH_2$ ) and oxygen ( $LO_2$ ) [1].

Thermal behaviour of such fluids are already well known on earth, which enabled, to build space launchers used in different space programs. However, some designers wish to know how these fluids behave in absence of gravity, to be able to use the launchers in space after being put off for a while, when the pipes are hot.

To answer this question, it is of prime importance to perform experiments at zero gravity. Several ways of getting the compensation of gravity can be used, as described in the background part below.

## 1.2 The study

In this master thesis, Nukiyama curves [2] are established to define boiling behaviours for different thermodynamics condition of  $LH_2$  and different level of gravity. These curves compare the evolution of the wall temperature due to an imposed flux. This study was made by using the magnetic compensation solution regarding the gravity problem.

To fulfil the needs, a specific cell has been built with an internal heater whose purpose is to transfer the desired power directly to the fluid. An observation system is installed to see, record and understand what happens. In the cell, a cooling circuit regulates the temperature around 20K, corresponding to the liquid hydrogen temperature at desired pressure (1 and 2 bars). It turns out that obtained results are very promising. This report present all the work I've done during this master thesis.

The first section of this report is composed of a background part, for the reader to understand the main aspects of this study. The next section is composed a presentation of different materials and methods that have been used. Results of this study are then presented before coming to the discussion part where several parameters are presented, and finally the last part concludes this master thesis.

## 2 Background

In this chapter, several aspects of the problem are presented, in order for the reader to be familiar with the main concepts of the thesis. First of all different techniques of getting microgravity are explained. A description of the magnetic compensation method is then presented, and finally an overview of thermal heat transfer in fluids is described

### 2.1 Classical techniques to obtain microgravity

Several techniques are nowadays utilized. All of them having their pros and cons. here is a brief review of these technique.

#### 2.1.1 Drop tower

The drop tower uses an inertial technique to compensate earth gravity. A freely falling body experiences gravity forces and an opposing inertial force, appearing due to the change of reference frame: from a Galilean frame attached to earth's surface to a non-Galilean frame attached to the body accelerating at the acceleration due to gravity. The result is that the body experiences zero g.

In drop tower, vacuum conditions are established, in order to reduce the aerodynamic forces. Experimental installations are put in shuttles falling down in the tower. By using this technique, it is possible to obtain a gravity of the order of  $10^{-5}$  g during 4 to 5 seconds.



Figure 1: Drop tower

It's difficult to increase this time, since on the one hand the height of the tower would

increase as the square of microgravity time and on the other hand, the resulting kinetic energy would be so large that a very huge brake system is required to dissipate this amount of energy . Moreover, the rotation of the earth itself should also be taken into account.

### 2.1.2 Parabolic flights

CNES and ESA have a modified plane called Airbus 0g, which enables to carry out some experiments in microgravity. This method enables to compensate gravity to the order of  $10^{-2}g$  during 20 seconds. A typical parabolic flight consists of about thirty parabolic trajectories. However, between two phases the plane has to go back to the previous elevation, during which an over gravity of 1.8g is applied on the plane. Moreover, such a technique is rather expensive and cannot be applied to  $LO_2$  and  $LH_2$  for safety reasons.



Figure 2: Airbus 0g

### 2.1.3 Space shuttle

Experiments could be conducted on space shuttle board when in orbit. In an orbit around earth on a reference frame fixed to the space shuttle, the centrifugal force cancels out gravity forces thus establishing zero g conditions. Typically gravity levels of the order of  $10^{-4}$  can be achieved.

### 2.1.4 Space station

Space stations, such as MIR erstwhile and the International Space Station enable to obtain a microgravity of the order of  $10^{-2}$  to  $10^{-3}$  g. The centrifugal force due to the rotation of the station around earth in an orbit is exactly in opposition to its weight. Residual acceleration due to human activities, vibration and constant repositioning to



Figure 3: Space shuttle

be kept in orbit induce oscillations (called jitter) and thus affect the quality of zero g obtained. However, the duration is much longer : a lab can be kept in microgravity during the whole life of the station (10 to 20 years).

### 2.1.5 Magnetic compensation

Zero g can be achieved by using strong magnetic fields through a technique called magnetic compensation. In this method the magnetic properties of the material to be levitated (diamagnetism /paramagnetism) are exploited to exert a strong magnetic body force in opposition to the gravity force. When sufficiently strong, the gravity forces can be cancelled to achieve zero g.

This is a very useful method to obtain microgravity since:

- The installation is on earth and immobile, exerting no space/mass constraints on the system, and could be easily secured against hazard risks related to  $LO_2$  and  $LH_2$
- Microgravity can be theoretically obtained for an infinite time duration.
- Several level of gravity can be achieved, to simulate for example the gravity conditions of other planets (such as Mars, Moon, etc...)
- Time variations of gravity are possible
- This technique is available anytime.
- The experiments can be less expensive than the other techniques of zero g, depending solely on the current in the coil (which can be considerably reduced by using superconducting coils)

This technique has however some drawbacks : volumes that could be levitated are small and the strong magnetic field may have some influence on the fluid one want to study.

## 2.2 Gravity compensated by a magnetic field

In this section, the basic principles of magnetic compensation are explained.

### 2.2.1 Principle

In order to compensate earth gravity for diamagnetic fluids, a magnetic field is applied. The interaction between this field and the fluid leads to a force per unit volume given by the following expression:

$$\vec{F} = \frac{\chi}{2\mu_0} \vec{\nabla} B^2 \quad (1)$$

where  $\chi$  represents the magnetic susceptibility of the fluid,  $\mu_0$  the permeability of the vacuum and  $\vec{B}$  the magnetic field, where  $\vec{\nabla}$  is the gradient operator. According to the magnetism convention,  $\chi$  is dimensionless. However, the mass susceptibility  $\chi_\rho$  or the molar one  $\chi_M$  is sometimes used in the literature.  $M$  is the molar mass.

The relation between these 3 values is :

$$\chi = \rho\chi_\rho = \frac{\rho}{M}\chi_M \quad (2)$$

The studied fluid is Hydrogen, which is a diamagnetic material. This kind of material is characterised by a very small, and negative susceptibility  $\chi$ . For liquid Hydrogen, it corresponds to  $(-10^{-6})$  whereas for its vapour phase it goes from  $(-10^{-9})$  to  $(-10^{-6})$ .

Eq (1) shows that this force exists only if

- there is a magnetic field
- this field varies in space

A volume element considered in a magnetic field is subject to two forces:

- its weight :  $\vec{F}_g = \rho \vec{g}$
- the magnetic force :  $\vec{F}_m = \rho \frac{\chi_\rho}{2\mu_0} \vec{\nabla} B^2$

By applying the fundamental principle of dynamics, it leads to

$$\vec{F}_m + \vec{F}_g = \rho \vec{g} + \rho \frac{\chi_\rho}{2\mu_0} \vec{\nabla} B^2 = \vec{0} \quad (3)$$

to simplify expressions, let's call the compensation vector  $\vec{G} = \vec{\nabla} B^2$ . Hence, by defining the vertical unit vector  $\vec{u}_z$  such as  $\vec{g} = -|g|\vec{u}_z$  and  $\vec{G} \cdot \vec{u}_z = G_z$  the exact magnetic compensation is obtained for :

$$\vec{G}_0 = \frac{-2\mu_0}{\chi_\rho} \vec{g} \quad (4)$$

Three remarks can be made:

- This expression shows that for diamagnetic material ( $\chi < 0$ ),  $G_0$  is oriented in the same direction as the gravity vector.
- To levitate a diamagnetic material such as hydrogen, huge field's gradient have to be applied. For comparison, a paramagnetic material such as oxygen, has a susceptibility  $10^3$  times higher than hydrogen, thus requires a smaller gradient to compensate gravity for the same volume
- the exact compensation for liquid Hydrogen at 20K is obtained for  $G_0 = -991.4T^2.m^{-1}$

### 2.2.2 Inhomogeneity of the compensation field

It is useful to define a new gravitational vector representing the effective compensation:

$$\vec{g}^* = \vec{g} + \frac{\chi\rho}{2\mu_0} \vec{G} \quad (5)$$

If the magnetic force is not applied  $\vec{g}^* = \vec{g}$ , which corresponds to the normal earth conditions. If the magnetic force is equal and opposite to the gravitational force, the residual gravity is null: the microgravity conditions are fulfilled.

The residual gravity can be considered as the effective gravity the fluid is subjected to. This method is adapted to compensate exactly tiny volumes. Indeed, the exact compensation is realised only at two specific points [3]. Since the gravitational force is constant at the scale of the installation, but the magnetic field is not, it leads to some non homogeneities of compensation: each point being subject to a slightly different gravitational vector.

A simple solenoid can create only two points where the gravity is exactly compensated. However, only one of these point is stable -i.e: if a small volume spreads from this point, it will automatically come back to its initial position, whereas for an unstable point it will tend to move further away (see explanation page 9).

To characterise the lack of compensation in the volume, it's useful to define the non homogeneity vector at each point:

$$\vec{e} = \frac{\vec{G} - \vec{G}_0}{|\vec{G}_0|} \quad (6)$$

This vector represents the residual forces applied to the fluid.

Mixing Eq (4),Eq (5)and Eq (6) leads to

$$\vec{e} = \frac{\vec{g}^*}{|\vec{g}|} \quad (7)$$

which can be analysed as the non dimensional residual gravity vector.

### 2.2.3 Magnetic compensation in a simple solenoid

#### 2.2.4 Vector analysis

With a simple solenoid, the geometry is axisymmetric and the induction vector  $\vec{B}$  and  $\vec{G}$  are defined only with r, in the radial direction of the coil and z components, in the axis direction. Hence, for our problem, one gets in cylindrical coordinates:

$$\vec{G} = \vec{\nabla} B^2 = \begin{pmatrix} \frac{\partial B^2}{\partial r}(r, z) \\ \frac{\partial B^2}{\partial z}(r, z) \end{pmatrix}$$

It leads to the following expression for  $\vec{\epsilon}$ :

$$\vec{\epsilon} = \frac{1}{G_0} \begin{pmatrix} G_r(r, z) \\ G_z(r, z) - G_0 \end{pmatrix}$$

Moreover, on the z axis, it leads to some interesting properties due to symmetry:

$$\vec{\epsilon}(0, z) = \begin{pmatrix} 0 \\ \frac{1}{G_0} \left( \frac{dB_z^2}{dz} - G_0 \right) \end{pmatrix}$$

Since a non-zero gradient is necessary to get the spatial compensation, zero g is possible only at the two extreme positions of the coil, where  $|G_z|$  is maximum as it can be seen in figure 4: These calculations have been carried out with the Levitation software developed by the High Magnetic Field National Laboratory (LNCMI) of the CNRS Grenoble.

For a specific material, a theoretical expression describes the relation between the magnetic field, the inhomogeneity level and the volume that can be levitated:

$$B = \frac{1}{2} \sqrt{\frac{3G_0 R}{2\epsilon_r + \epsilon_z}} \quad (8)$$

This expression is given by considering the second order Taylor expansion of  $\vec{B}$  in the expression of  $\vec{\epsilon}$  and using Maxwell equations :  $\text{div}(\vec{B})=0$  and  $\text{rot}(\vec{B}) = \vec{0}$  and considering a vertical magnetic field. R corresponds to the characteristic length of the levitated volume (in m)

For example, to levitate hydrogen, a magnetic field of 5.5T can compensate gravity with a residual level of 1% for a radius of 1.22 mm, which corresponds to a volume of  $7.6\text{mm}^3$  of hydrogen

The line drawn in figure 4 represents the compensation  $G_z$  for hydrogen. It can be easily seen that only 2 points can be compensated. Since the magnetic field depends directly on the current flowing through the coil, three configuration can be presented:

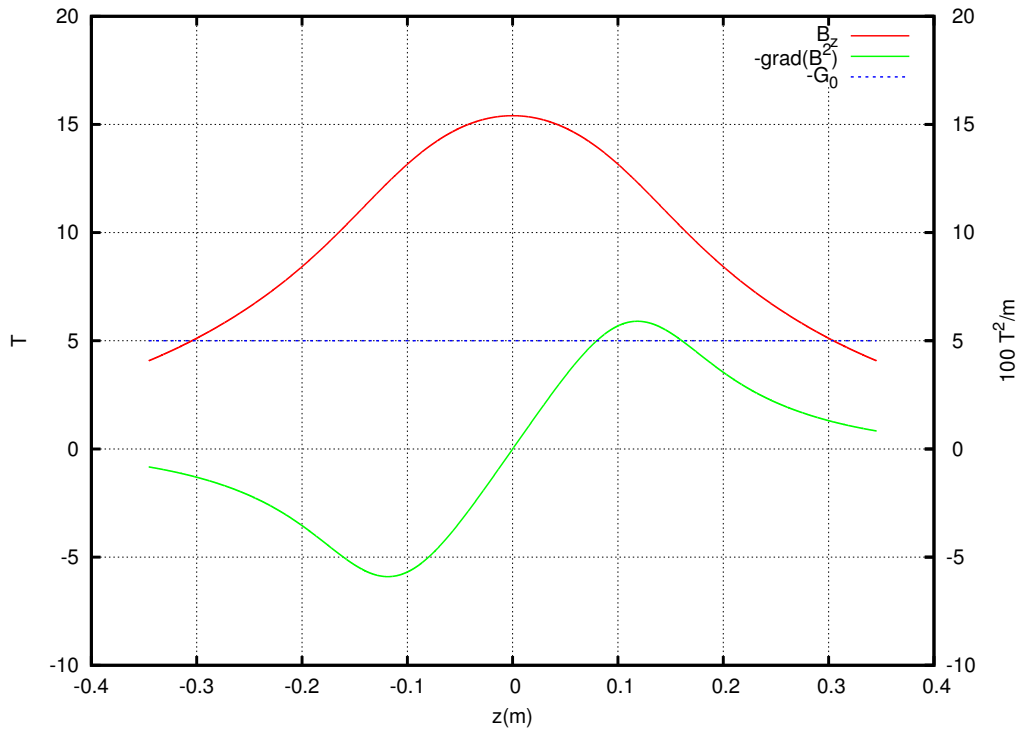


Figure 4: Magnetic induction  $B_z$  and Compensation  $G_z$  on  $z$  axis of the coil for Hydrogen

- if the current is not high enough, the  $|G_z|$  curve doesn't cross the compensation line: there is no compensation at all
- if the current increases until the  $|G_z|$  curve becomes tangent to the compensation line, there is exactly one compensation point
- if the current increases even more, there are two compensation points

The third configuration is the only one which is interesting to compensate the gravity in a volume. The part where the curve is above the compensation line is called the overcompensation zone, whereas when the curve below this curve is called the undercompensation zone. It can be noticed that the green line corresponds to the opposite of the gradient. That's why it's inverted compared to figure 5

### 2.2.5 Axial stability

The major difference between a paramagnetic and a diamagnetic fluid is the sign of the vector  $\vec{G}$  due to the contribution of the magnetic susceptibility. Hence, to compensate the gravity in a paramagnetic fluid,  $\vec{G}$  has to be positive in order to get a magnetic force upwardly oriented (if the gravity is down oriented) whereas for diamagnetic fluid,

such as hydrogen,  $\vec{G}$  has to be negative since  $\chi_m$  is negative too.

There are only two forces acting on a bubble: upthrust buoyancy and the magnetic force. For each fluid near its compensated area, two cases are possible as it can be seen in figure 5:

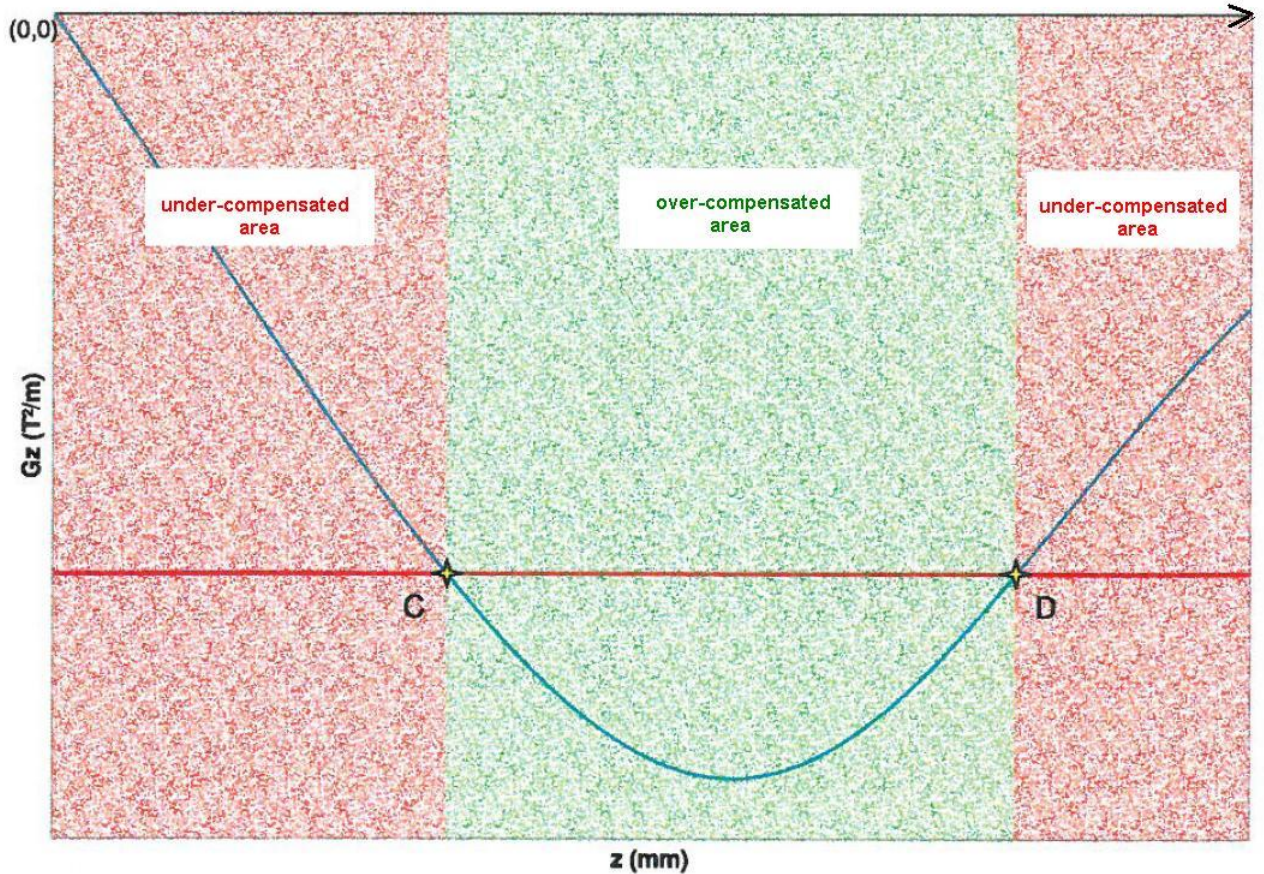


Figure 5: Stability of magnetic compensation for diamagnetic fluids

- The bubble is at C: a small upward displacement (right side on the  $z$ -axis of figure 5) puts the bubble in the overcompensated area, the gravity becomes lower leading to a smaller upthrust buoyancy. The resulting force tends to move the bubble down, back to C. If the small displacement is directed in the other way, the bubble would be in the under-compensated zone, where the gravity becomes higher, leading to a stronger upthrust buoyancy. The resulting force tends to move the bubble back to C. This point is stable for vapour since whatever the displacement, the bubble come back to it's initial position.
- The bubble is at D: a small upward displacement put the bubble in the under compensated area, where the upthrust buoyancy is stronger than the magnetic

force, the resulting force tends to move the bubble even upper. If the small displacement is directed in the other way, the bubble would be in the overcompensation zone, where the gravity is lower, leading to a smaller buoyancy. The resulting force tends to move the bubble even lower. This point is unstable for the vapour phase.

It can be noticed that the unstable point for vapour phase D is stable for liquid phase and the stable point for vapour C phase is unstable for liquid phase: for vapour the magnetic force is directed downward to compensate the buoyancy (the weight of vapour is negligible) and for liquid it's directed upward to compensate the weight

### 2.2.6 Radial instability

according to (7)

$$\vec{g}^* = g \begin{vmatrix} \epsilon_r \\ \epsilon_z \end{vmatrix}$$

thus

$$\epsilon_r = \frac{G_r}{G_0} \quad (9)$$

That is why the study of  $G_r$  enables to determine the radial force applied on a bubble. A simple Taylor expansion at first order shows that  $\epsilon_r$  is proportional to  $r$ . Hence, if a small displacement deviates the bubble from the  $r$ -axis, we get:  $G_r > 0$ , leading to  $\epsilon_r < 0$  since  $G_0 < 0$  and finally  $g_r^* < 0$

Hence radial acceleration  $g_r^*$  is oriented to decreasing  $r$ , thus the resulting upthrust buoyancy is oriented to increasing  $r$ . That's why hydrogen is radially unstable

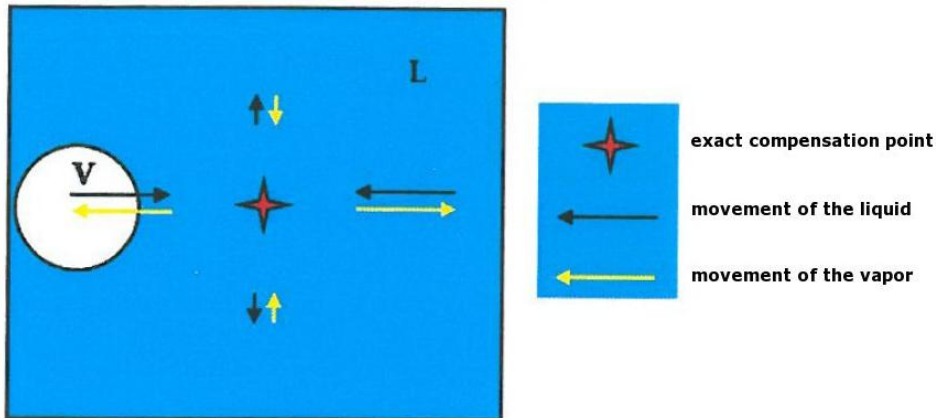


Figure 6: radial instability of an hydrogen bubble

### 2.2.7 Modification of the gravity level

Lots of combinations of current ( $I$ ) and axial position ( $z$ ) are possible. Let  $(I_0, z_0)$  be one such combinations.

By projecting Eq(5 ) on z axis, it leads to:

$$g = g^*(I, z) + \frac{\chi_\rho}{2\mu_0} G_z \quad (10)$$

where  $G_z(I, z) = \frac{dB^2}{dz}(I, z)$  and  $g^*$  is the residual gravity,  $g$  the earth gravity,  $\chi_\rho$  the mass susceptibility of hydrogen, and  $\mu_0$  the magnetic permeability of vacuum and  $G_z$  the axial component of the magnetic compensation force.

By definition, we get  $g^*(I_0, z_0) = 0$  , hence

$$g = \frac{\chi_\rho}{2\mu_0} G_z(I_0, z_0)$$

The presence of a metallic insert could have change the shape of the magnetic field. However, in our case no metallic insert is added and thus the magnetic field is directly proportional to the current in the solenoid. that is why

$$\frac{\chi_\rho}{2\mu_0} G_z(I, z) = I^2 \cdot f(z)$$

with f and function independent of the current. Hence it leads to

$$g = g^*(I, z) + \chi_\rho I^2 \cdot f(z) \quad (11)$$

and

$$g = \chi_\rho I_0^2 \cdot f(z_0)$$

If now the altitude  $z_0$  is kept constant , the relation becomes

$$g = g^*(I, z_0) + \chi_\rho I^2 \cdot f(z_0)$$

Since

$$\frac{g}{I_0^2} = \chi_\rho f(z_0) ,$$

$$g = g^*(I, z_0) + I^2 \frac{g}{g_0}$$

It finally gives the relation between the current and the residual gravity :

$$\frac{g^*(I, z_0)}{g} = 1 - \left(\frac{I}{I_0}\right)^2 \quad (12)$$

or

$$\frac{I}{I_0} = \sqrt{1 - \frac{g^*(I, z_0)}{g}} \quad (13)$$

This relation will be useful to know the applied current corresponding to the desired level of gravity.

## 2.3 Heat transfer in boiling fluids

### 2.3.1 Three modes of heat transfer

There are three fundamental mechanisms of heat transfer : conduction, convection and radiation.

#### Conduction

This mode corresponds to a transfer of heat in a material without any physical movement of material. Fourier's law gives the heat flux density  $\vec{q}_{cond}$  in  $W.m^{-2}$  transmitted by this phenomenon:

$$\vec{q}_{cond} = -\lambda \vec{\nabla} T \quad (14)$$

where  $\lambda$  (in  $W.m^{-1}.K^{-1}$ ) is the thermal conductivity of the material and  $T$  (in K) is the temperature field.

#### Convection

For this mode, the heat transfer is due to a movement of particles. In the general case, the heat flux density transmitted by convection from a solid bulk to a liquid is given by

$$\vec{q}_{conv} = h(T_b - T_f) \vec{n} \quad (15)$$

where  $h$  (in  $W.m^{-2}.K^{-1}$ ) is the convection exchange coefficient,  $T_p$  (in K) is the temperature of the solid wall,  $T_f$  is the temperature of the fluid far away from the solid and  $\vec{n}$  the normal vector to the solid directed outward.

The transfer coefficient  $h$  depends strongly on the configuration of the system. Two different types of convection are distinguished: the natural convection, where the system is put in a force field, such as gravitational force, or forced convection where the fluid is put in motion through external forcing via another system, a pump for example.

#### Radiation

The heat flux density  $\vec{q}_{rad}$  emitted by a system at a certain temperature  $T$  is given by

$$\vec{q}_{rad} = \epsilon \cdot \sigma_B \cdot T^4 \cdot \vec{n} \quad (16)$$

with  $\epsilon$  the emissivity of the system,  $\sigma_B = 5.6703 * 10^{-8} W.m^{-2}.K^{-4}$  the Stefan-Boltzmann constant,  $T$  (in K) the temperature of the system and  $\vec{n}$  the normal vector of the system directed radially outward

### 2.3.2 Boiling

Boiling happens when the ambient pressure is larger than the vapour pressure. It is a very effective way of heat transfer. Two boiling type exist [4]:

- The homogeneous one, where the fluid is boiling in all the liquid. This type is very difficult to achieve experimentally
- The heterogeneous one, where the fluid is boiling in contact to a hot wall, in a different material than the studied fluid.

The experiment that have been carried out in this master thesis have been done with this second type. Extreme care has been taken to ensure that :

- The fluid is pure
- The liquid is in equilibrium with its vapour or undercooled.
- The volume is closed
- The heating heat flux was given by a solid material

There are two different forms of boiling that will be further explained in the next part : nucleate/pool boiling, and film boiling.

#### Pool boiling

To study pool boiling, two different types of experiment are carried out, presented in figure 7:

- using a hot wire [5]
- using a heating flat plate

Our experiment have been carried out with the flat plate mode. The heating part is a hot wall placed in the bottom of the cell in which the fluid is filled. In normal condition, due to gravity, the liquid is at the bottom part of the cell while the vapour is above it. The heating surface is then totally in contact with the liquid.

Dividing the power injected in the liquid by the area of the heating plate gives the heating flux density.

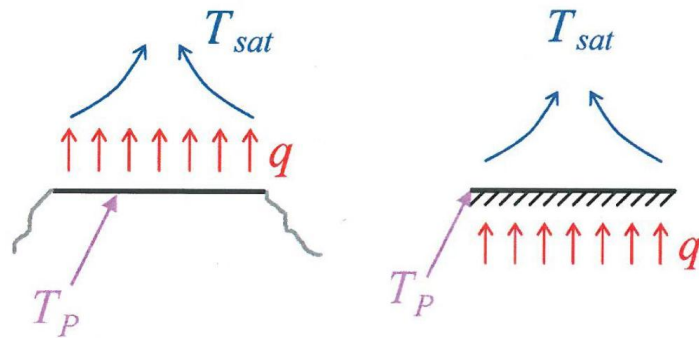


Figure 7: experimental devices : hot wire (on the left) and plat plate (on the right)  $T_{sat}$  is the saturation temperature of the fluid

### 2.3.3 Nukiyama curve

Several parameters can be measured: the heat flux density  $q$  (in  $W.m^{-2}$ ), the saturated temperature of the fluid  $T_{sat}$  and the temperature of the wall,  $T_p$ . The heat flux density  $q$  is imposed and the temperatures are measured. Each experimental point is recorded in stationary regime, when all parameters are stables. The overheating is defined as  $\Delta T_{sat} = T_p - T_{sat}$ . The curve  $q=f(\Delta T_{sat})$ , called Nukiyama curve can then be plotted (see figure 8)

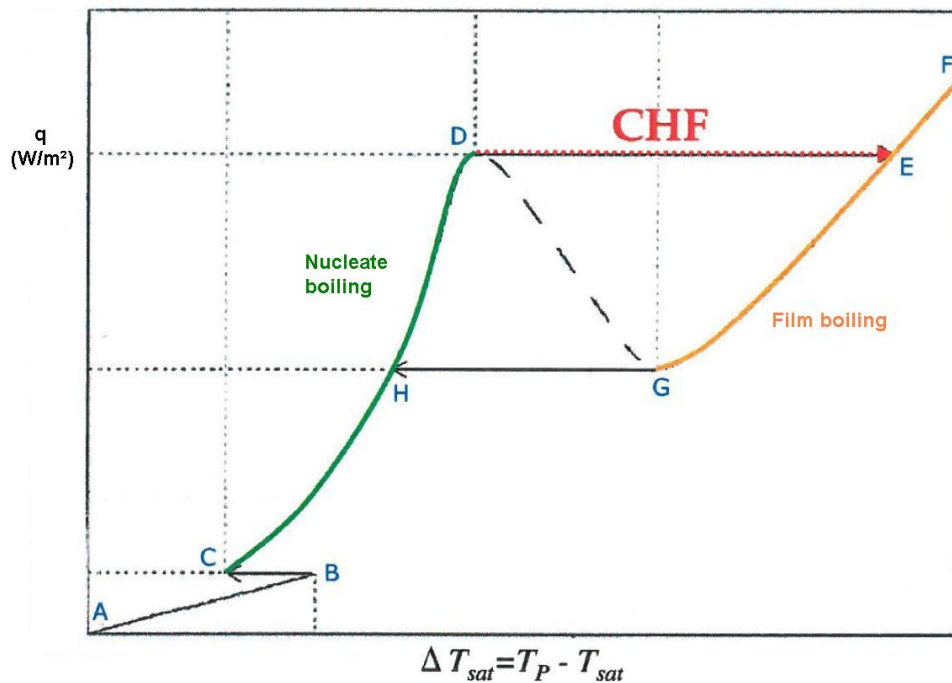


Figure 8: Nukiyama curve

This curve starts when the fluid is at saturated temperature ( $\Delta T_{sat} = 0$ ), where the imposed heat flux is null.

### From A to B

In the first region, there is no vaporization. The temperature of the fluid in contact with the heater is below the boiling point of the fluid. There is only conduction and natural convection in the fluid. The heat flux is transmitted directly to the liquid very slowly by a conduction process first and then by a convective one. From B to C it's the onset of nucleate boiling.

### From C to D

As soon as the overheating achieves the threshold at B, that is when the temperature of the first layer of liquid in contact with the heater is equal to the boiling point, bubbles appear. As it can be shown in the graph, the temperature of the wall strongly decreases when **the nucleate boiling** starts (B-C), due to the latent heat of vaporization: Since this phase change is endothermic, it absorbs heat while creating bubbles. This boiling continues until reaching the point D. Even if the heat flux constantly increases, the overheating is quite small (i.e., the wall stays quite cold), due to the efficiency of this thermal transfer. As the heat flux is increased more and more bubbles are created (figure 9).

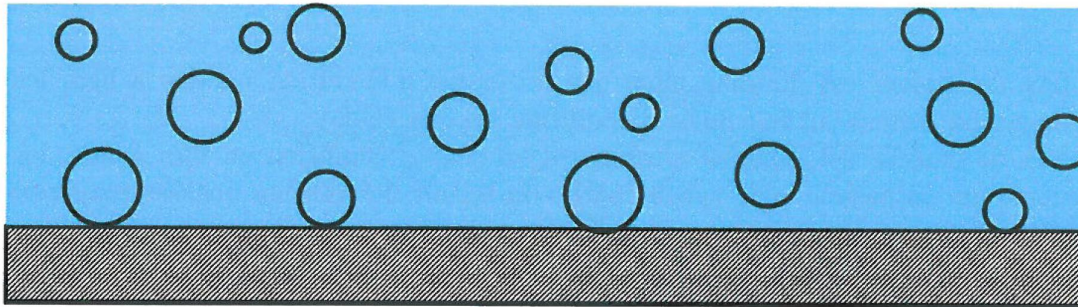


Figure 9: Nucleate boiling.

### From D to E

As soon as the threshold D is achieved, the heat flux is too large to be evacuated and for the nucleate boiling to keep going. The corresponding flux is called CHF (**critical heat flux**). There is so much vapour that the liquid can't reach the wall to cool it: a vapour film constantly covers the wall (figure 10).

Thermal transfer is highly impacted by this vapour layer as it has low thermal conductivity. The temperature of the wall ( $\Delta T_{sat}$ ) quickly increases and reaches a very different

equilibrium value, even if the heat flux stays constant.

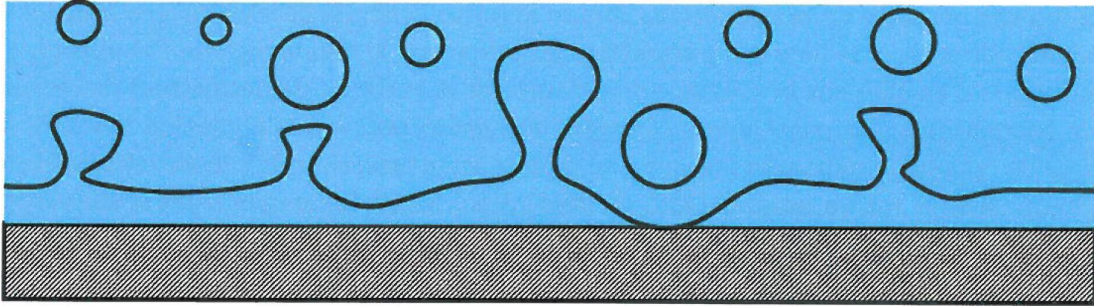


Figure 10: Film boiling.

### From E to F

It is **film boiling**. When the heat flux is still increased, the wall temperature keeps increasing with a quite high temperature. The slope of the curve is very small, meaning that the thermal transfer is very poor: a small increase in the flux causes a huge increase in the wall temperature. If the heat flux is sufficiently high, the material can reach its melting point and then destroy the wall (in F).

There is an hysteresis:

- If the heat flux decreases during the nucleate boiling phase, experimental points stay in the nucleate boiling part of the curve
- If the heat flux decreases during the film boiling phase, experimental points don't come back to the nucleate boiling curve but stay in the film boiling one (F-G)

There is a minimal heat flux that can be reached in film boiling (G). At this point, the liquid starts to wet the wall again and then the nucleate boiling phase can be re-established.

### From F to G

This part of the curve is very difficult to obtain due to the instability of the change between the two modes, and cannot be achieved with this method. To get it, the overheating has to be imposed, not the heat flux.

This boiling curve is universal. Whatever the studied compound, the shape of this curve is the same. This thesis will be focused on the plotting of this curve for liquid hydrogen for different pressures and levels of gravity.

### 2.3.4 Nucleate boiling

To start boiling, an energy threshold has to be crossed. The temperature of the heater brings the needed amount of energy to do it. However, several other parameters also play important role in it, especially surface defects, which can considerably reduce the threshold. That's why the needed energy to start boiling on a polished surface is higher than on a rough one [4].

Each defect is a potential nucleation site, where bubbles will be able to develop. It's a geometrical imperfection (hole), containing vapour or air. While the threshold is crossed, this site become active and bubbles start to nucleate from it. Different shape of site leads to different behaviour of boiling [6].

There are several steps in the creating of bubbles:

- waiting
- inertial growing
- thermal growing
- leaving

the following figure show this different steps.

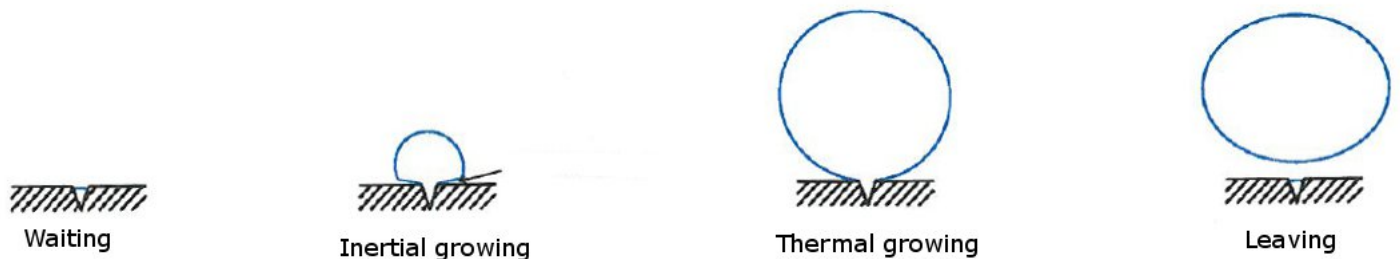


Figure 11: developement of a bubble

#### Waiting

A small volume of vapour stays in the nucleation site. The liquid phase, at saturated temperature, recovers this site, replacing the area occupied by the previous bubble. The heating compound heats up the liquid by conduction. During this step, the bubble doesn't grow.

#### Inertial growing

As soon as the thermal limit layer is built back, the overheating becomes sufficient for a new bubble to start growing. Pressure forces are then higher than the surface

tension, leading to the fast development of the bubble with an hemispherical shape. the micro layer between the bubble and the wall enables to improve the heat transfer by evaporating the liquid caught in it.

the bubble grows according to the Rayleigh-Plesset model [7] with a characteristic speed:

$$\frac{dr_b}{dt} = \sqrt{\frac{2\Delta P}{3\rho_L}} \quad (17)$$

where  $r_b$  is the radius of the bubble,  $\Delta P = P_v - P_L$  is the pressure difference between the liquid and gas phase,  $\rho_L$  is the liquid density, and t the time.

### Thermal growing

As soon as pressure forces are of the same order of magnitude as that of the surface tension, the bubble gets a spherical shape, to minimize its energy. Its growing is due only to the vaporization of the liquid at the interface. Heat transfer is then done only by diffusion at the interface and grows as [7], even if a small flow is present:

$$r_b \propto \frac{\Delta T}{\rho_v \cdot H} \lambda_L \sqrt{\frac{t}{D_{T,L}}} \quad (18)$$

where  $\lambda_L$  is the thermal conductivity of the liquid phase,  $\Delta T$  is the overheating,  $\rho_v$  is the liquid density, H is the latent heat of vaporization, and  $D_{T,L}$  is the thermal diffusivity of the liquid phase. This expression is correct only in a hot liquid, far away from the wall.

### Leaving

As soon as the bubble is as long as the capillary length,

$$r_b \sim \sqrt{\frac{\sigma}{g \cdot \Delta \rho}} \quad (19)$$

where  $\sigma$  is the surface tension, g the gravity and  $\Delta \rho$  the difference of density between the liquid and gas, the bubble leaves due to upthrust buoyancy. It brings some saturated liquid with it, leading to a perturbation in the thermal boundary layer. A new cycle can then start again.

### **2.3.5 Critical Heat Flux**

As explained above, the heat transfer is more intense in nucleate boiling than in film boiling. Moreover, the hotter the wall, the better the transfer. Hence, it's very important for an industrial heat transfer device to work on C-D part of Nukiyama curve, close to point D.

However, this point shouldn't be crossed, otherwise it would heat up the wall due to low conductivity of the the vapour layer. The transition occurring at CHF is, by definition, critical: it's instantaneous, unstable, chaotic and irreversible (even if the heat flux is decreased directly after having crossed this point).

A lot of experiments have been done since the discovery of the CHF, trying to understand this phenomenon. However, even if lots of configurations have been studied, industrials are dependent only on empirical data. Hence they have to apply a quite important security coefficient to size their installations. Knowing exactly what happens would reduce this coefficient and then costs.

This background section has presented a brief overview of concepts that are necessary to understand and treat the subject of this master thesis

## 2.4 Information about hydrogen

Hydrogen gas can be considered as an ideal gas. It is a colourless, odourless, tasteless, non-toxic, non-corrosive, non-metallic diatomic gas at standard pressure and temperature. Its density is very low, which makes it necessary for any practical applications to either compress the hydrogen or liquefy it. Figure (12) shows its phase diagram

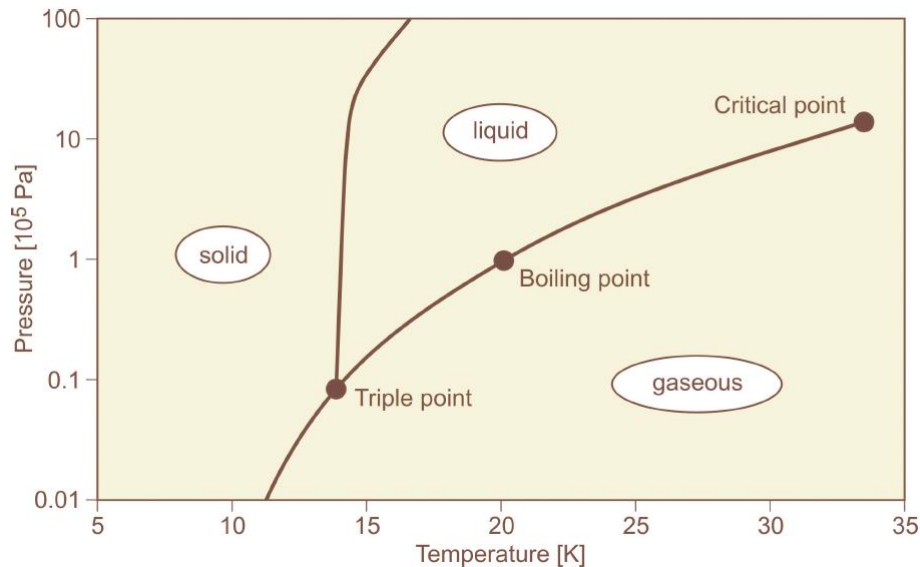


Figure 12: Phase diagram of hydrogen

As shown in the diagram, at 1 and 2 bar, the corresponding phase change is around 20K. That is why cryogenic installation is necessary to carry out our experiments.

It is an highly diffusive and highly buoyant gas, which mixes with air very quickly upon release. Hydrogen coexists in two different forms, ortho and para hydrogen, the fraction of each of these components depends on the temperature. Normal hydrogen at room temperature is 75% ortho (nuclear spins aligned) and 25% para (spins anti-aligned). At 20 K, there are 99.821 % of para and 0.179 %ortho . It takes 3-4 days until a new equilibrium state is reached.

However, magnetic impurities and also small oxygen concentrations are able to catalyse ortho-para conversions raising the rate by several orders of magnitude to the order of hours. Catalysts such as  $Fe(OH)_3$  or even small concentration of oxygen can accelerate this transformation and/or enable to get a desired fraction of each.

There are only few differences between physical properties of the two spin states. The most important one is their large energy difference which results in major differences for the specific heats and thermal conductivities.

### 3 Methods and materials

In this section, the whole installation is described. First, an explanation about different functions of each component is given, and then the sizing of some of them is presented.

#### 3.1 The experimental setup

The installation is called LHYLA (Liquid HYdrogen Levitation Apparatus). A sketch of it is presented below on figure 13. It shows the different parts of the installation, which are precisely described later on.

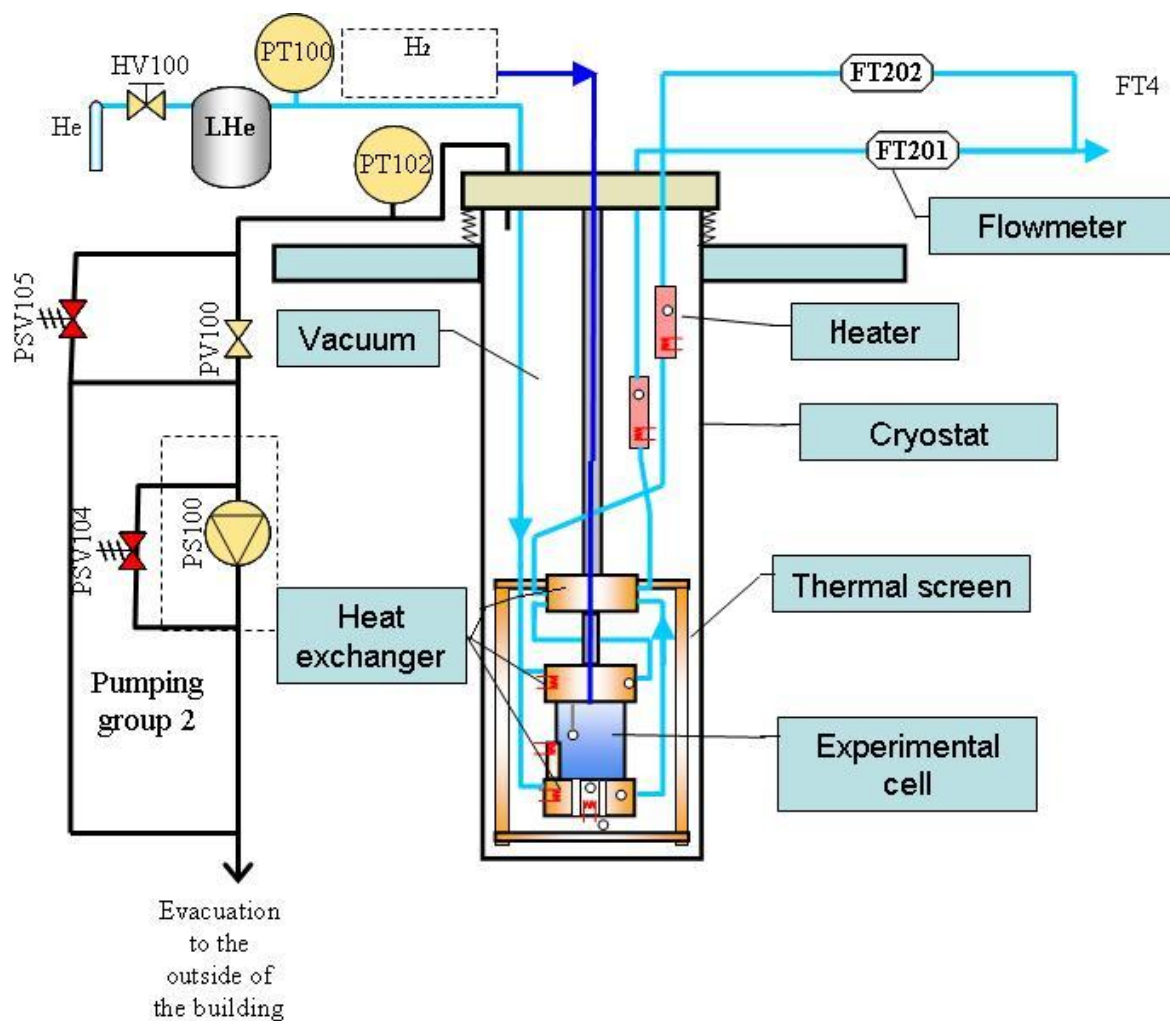


Figure 13: Global drawing of the installation

It can be noticed that the vision system is not represented on this figure, but is presented later.

### 3.1.1 The cryostat

The creation of undesired ice is the main enemy of cryogenists. Indeed it could break down a whole installation. Whatever the substance, if its solidification temperature is higher than the colder part of the installation, it could create ice.

That is the reason why cryogenics is always associated with vacuum technique: it prevents from having undesired elements, and also removes convection movements in the cryostat which would impact the cooling by adding this thermal transfer to others.

To cool down an installation, the heat has to be extracted. It can be done either by direct or indirect technique. The first one consists in directly extracting the heat of the device by thermodynamic cycles, and the second one consists in using cryogenic fluids such as liquid helium or nitrogen for example, to extract heat from the device.

The first method is much more expensive than the second one. That's why for our purpose, the second one has been chosen.

The cryostat is the compound which enables to thermally isolate the low temperature device (fluid and mechanical parts) to the external atmosphere.

Our cryostat is represented in figure 14:



Figure 14: Moving of the cryostat with an overhead crane

As shown it's a quite large structure (3m high) which can be manipulated only

with overhead crane. Such a set up is designed to study both ergol components of any rocket engine, i.e.  $LO_2$  and  $LH_2$ . As explained before, the microgravity zone for  $LH_2$  is situated at the top site of the levitation coil; while in the case of  $LO_2$ , this zone is at the bottom of the coil.

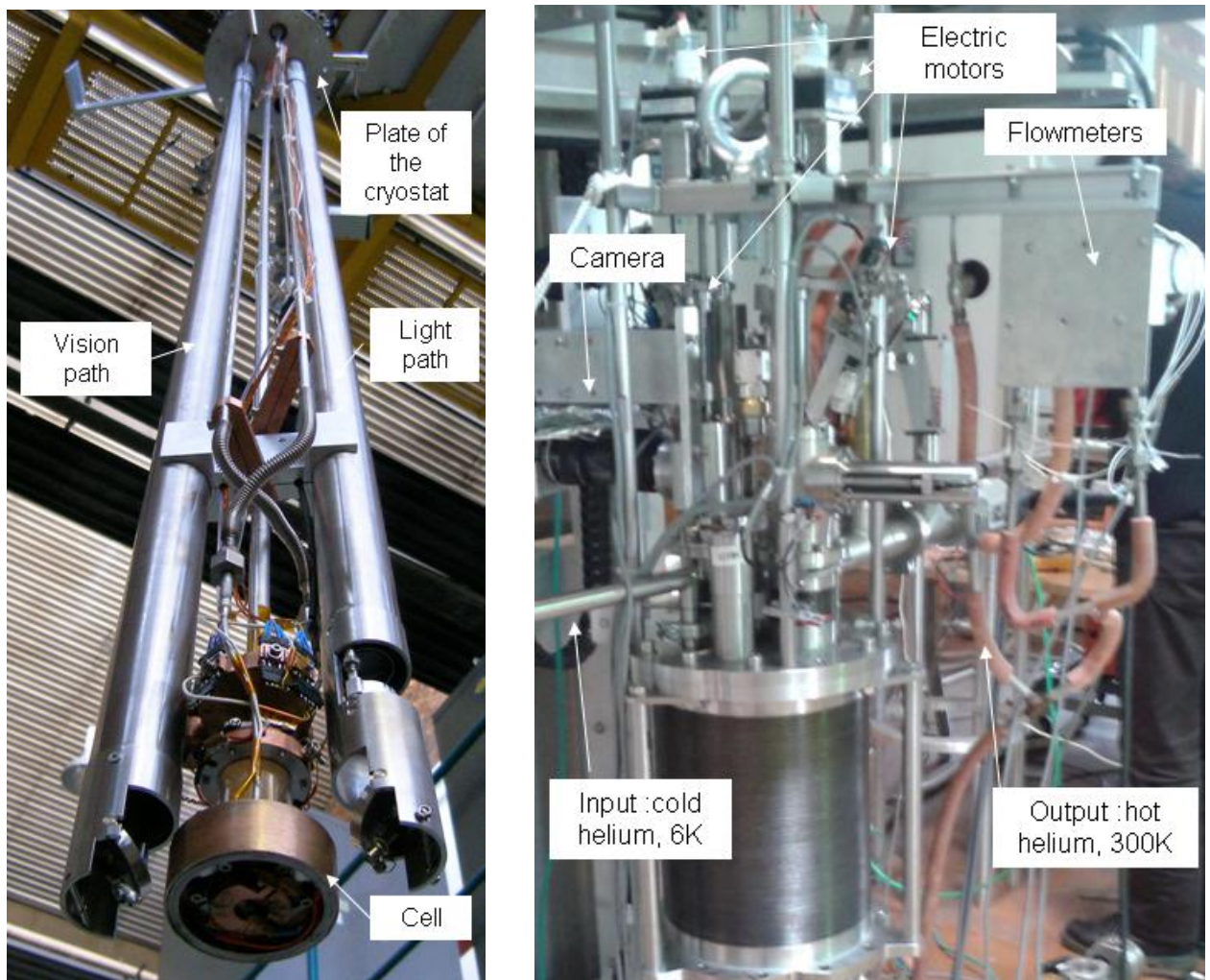


Figure 15: Inside of the cryostat (on the left) and top of the cryostat(on the right)

To limit heat exchanges inside the cryostat, the three modes already presented are utilized:

- Convection: A secondary vacuum ( $10^{-5}$  mbar) is maintained inside it by a turbo-molecular pump. This prevents from any gas exchange.
- Conduction: Thanks to the secondary vacuum, heat losses by conduction are only possible through metallic pipes going from top of the cell (endoscope, gas feeding). However, they are very long and thin and then the heat transfer is insignificant(it will be precisely expressed in the sizing part).

- Radiation: a thermal shield (not represented on the previous figure) totally surrounds the experimental cell. It is cooled by gaseous helium and achieves a temperature around 40 K. Hence it reduces a lot radiating heat transfer (from 5W to some mW)

To see what happens inside the cell, a vision system is installed, as shown in figure (15). This system is further described. The flange situated on top of the cryostat (see figure 15) contains:

- 2 electrical motors for the rotation and translation of light and vision mirrors
- 2 electrical motors for the translation of light and vision endoscope
- Electrical connection of sensors and heating resistance
- Cooling pipes: cold helium at 6K enters into the cryogenic path system to regulate the  $LH_2$  temperature and exit at 300K to avoid any ice on the set up.
- A camera enables to see and record what happens into the cell. everything is recorded.
- Flowmeters enable to control precisely the helium flow into the cryogenic circuit. However, they need to work at ambient temperature, that is why an heaters are placed before them , to set gas helium at room temperature.
- A movable system that allows to check the  $LH_2$  temperature along the vertical axis of the cell and to verify that one remains in isothermal conditions during the experiment is also installed. It is basically composed of rack and pinion.
- A safety valve is also installed in the system. If the cell explodes, hydrogen is then released into the vacuum of the cryostat, leading to a strong pressure increase. Then the valve is automatically opened and the hydrogen is exhausted to the outside of the building.
- A connection to the pumping system

## Mechanical description of the cryostat

The vacuum vessel of the cryostat is made of stainless steel 304L. It has been formed by boiler manufacturing. It is only 1 mm thick. That's why there are several reinforcements installed all over its entire height to prevent from crashing when making vacuum inside. Its volume is around 430 L and the medium diameter is 185 mm.

A flat flange closes the cryostat. On the one hand, it mechanically supports all compound inside the cryostat as already mentioned and on the other hand it ensures airtightness between the inside and the outside of the cryostat.

For electrical connection, Jaeger plugs are installed, enabling a simple and ergonomic access to the installation during maintenance.

Both endoscopes can be manipulated independently one from the other. They are activated by electric motors controlled by a supervision panel on the computer.

Mirrors are placed at the end of each endoscope. They are linked by cables which can be pulled by step by step motor to adjust their angular position. A spring is also installed in order to set the mirror back in position while keeping the cable free.

Lighting endoscope has a removable frosted mirror, which enable to go from parallel to diffuse light. It can be activated by a switch on top of the cryostat.

The diameter of endoscopes is  $D_{endo}=40$  mm and they are almost 2 m high. Hence, according to Eq (20) and (21) below, for a wavelength ranging from 400 and 800 nm, the smallest detail that can be seen is around 25-50  $\mu\text{m}$

### **3.1.2 The observation system**

The experimental cell is enclosed in the cryostat. Since everything is metallic, it is opaque, which makes the direct observation of the cell from the outside impossible. That is why an optical system is installed from the top flange. There is a light source (white light) whose the intensity can be modulated and a CCD camera with special lens to catch pictures. The observation is done by transmission of the light through the cell.

## Endoscopes

Since the camera and the lighting system are far away from the cell, an optical system had to be built for the light to follow a certain path, going from the lamp, through the cell and reaching the camera. An optic fiber guides the light path through the lighting endoscope until it reaches the cell. Before this, light rays going out of this fiber (and thus considered as punctual source) are going through several lenses for the light to diffuse in a parallel manner.

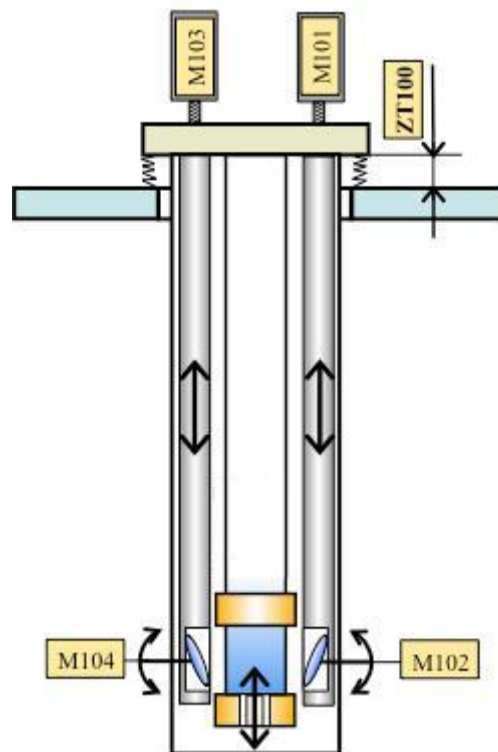


Figure 16: Observation system

## CCD camera

The camera is placed on the top flange of the vision endoscope to get the rays that are going out from the cell. A magnification objective is added for the rays to cover enough surface on the CCD sensor.

The capture system is composed of :

- an analogous and monochromatic CCD camera (Watec-902B)
- a clock overlay (for date and time)

- a VCR (video cassette recorder) to VHS tape.
- a printer to get an instant printout
- a normal definition screen (SD)

All components are plugged in serial by RCA or BNC wires. The resolution is 768x494. The main advantage of this system is its quite simple installation. As soon as it is switched on, an image appears. However, post-processing of recordings are quite complex since it requires a numerical conversion. The poor resolution of recording doesn't prevent from doing very sharp picture analysis. The camera is associated with a 70 mm focal length objective with a focal doubler. Hence it's a 140 mm focal length.

### Angular resolution

Observation via an endoscope creates an alteration in quality of the real situation. The diffraction limits the angular resolution through the following formula:

$$\theta \approx 1,2 \frac{\lambda_l}{D_{endo}} \quad (20)$$

where  $\theta$  is the maximal resolution power,  $\lambda_l$  (in m) the wavelength of the light, and  $D_{endo}$  (in m), the diameter of the endoscope, corresponding to the numerical aperture. Since  $\theta$  is small, it leads to :

$$\tan\theta \approx \theta \approx \frac{l}{L_{endo}} \quad (21)$$

where  $l$  (in m) is the size of the smallest element that can be seen by this system and  $L_{endo}$  the length of the endoscope.

### **3.1.3 The experimental cell**

There are several prerequisites to build an experimental cell for study of thermal transfer in microgravity:

- It has to be transparent to be able to see what happens in there
- It has to be regulated in temperature
- It has to contain an heating component to apply an heating flux to the fluid
- No leakage are allowed

That is the reason why the cell is built as presented on figure 17. A transparent sapphire cylinder of 30 mm diameter is bridled at each side by one heat exchanger made of copper material. Heating resistances enable to regulate the temperature of the cell. Another advantage of the sapphire is its good conductivity at 20K. Its mechanical properties, such as tensile elastic limit, are compatible with the maximum possible pressure that are used.

Stainless steel has very good mechanical properties, but poor thermal ones. It's a material often used in cryogenics. Unfortunately, its magnetic properties are disappointing. For our purpose, this very small interaction between material and magnetic field is totally advantageous.

Heat exchangers are made of copper for better thermal conductivity. Other mechanical pieces are made of stainless steel 304L, except for the inner ring presented below on figure 17 which is in titanium.

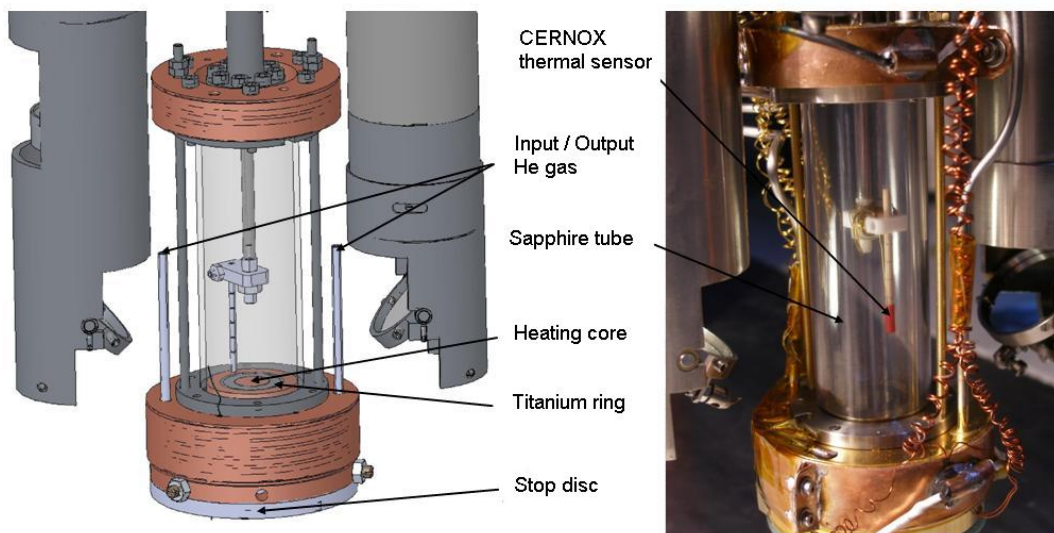


Figure 17: Modelisation of the cell (on the left) and real cell (on the right)

Titanium is chosen for this ring to thermally insulate the heating part from the bottom of the cell. It's a ring 100  $\mu\text{m}$  thick, shown in figure 18. The sealing of the cell is done with Indium seals. This has several advantages: on the one hand, it doesn't become breakable at the temperature achieved by our experiment (20K) and it is inert with hydrogen. On the other hand, it's very easy to shape it the needed way. As soon as it is installed, two clamps are squeezed.

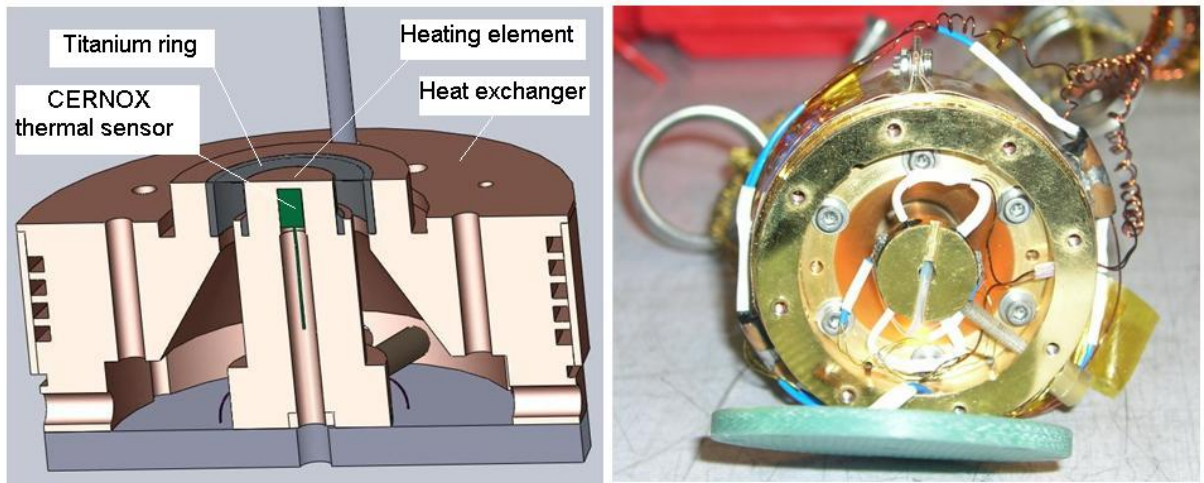


Figure 18: section of the bottom of the cell (on the left) and picture of the bottom of the real cell (on the right)

The cell itself (inside the sapphire) has a diameter of 30 mm and is 100 mm high. This cell was used for previous experiments with liquid oxygen. That's why all copper elements have been recovered by a very thin layer ( $1\mu\text{m}$ ) of gold.

### Regulation of the temperature

Heat exchangers have been machined into the clamps (see fig 18). To carefully regulate the temperature, the technique utilized in our apparatus is to set a helium gas flow inside heat exchangers situated on both sides of the sapphire tube. As it has been experimentally observed, the temperature regulation is much better with gas helium than with liquid helium.

The helium flow rate in each exchanger is imposed by the operator. As shown in figure 13, the fluid arrives in a single pipe and is divided into the two ways near the cell. Heating resistance of about  $100\ \Omega$  are installed in each heat exchanger. Thermometers are constantly measuring the temperature of each of them. Their precision is about  $0.01\text{K}$ . The regulation is done by the Programmable Logic Controller (PLC) , which does a PID type regulation.

### Application of an heat flux

At the center of the cell bottom flange, an heating resistor is installed inside the copper piece, enabling to heat it up only via Joule effect (see fig 18). Its exchange surface is  $1\ \text{cm}^2$ . As explained above, this piece is thermally insulated from the rest of the exchanger with the titanium ring. The electrical generator gives  $15\ \text{W}$  to the resistor, which is sufficient since the theoretical heat flux is around  $12\ \text{W}\cdot\text{cm}^{-2}$  [2] at normal temperature and pressure.

### 3.1.4 Thermal sensors

To measure the temperature of the cell, there are several cryogenic CERNOX sensors. The heating element and each exchanger are equipped with such sensors. This thermometer is made of resistance whose value is proportional to the temperature. Hence, to determinate the temperature, it's only necessary to measure the resistance and to associate the corresponding temperature value. Measures are 4-wire type: since errors due to resistance variation of the wire are reduced compared to a 2-wire type measure. The electrical connexion is then ensured by 4 wires with a diameter of 0.2 mm in manganin ( 86% copper, 12% manganese, and 2% nickel.). This material has been chosen thanks to its virtual zero temperature coefficient of resistance value and to minimize heat transfer between point that need electrical connections.

Thermalisations are installed on the cold piece to limit even more the conduction thermal transfer.

### 3.1.5 The magnetic map

After having seen the material itself, it is interesting to detail the surrounding of the experiment, and especially the magnetic field resulting from the coil.

A magnetic map has been established by using the software 'Levitation' developed by the LNCMI. It uses a taylor expansion of the magnetic field to establish such a map. The figure 19 below shows the residual gravity vector present in the considered volume, resulting from Eq (5) and Eq (6).

The different curves correspond to the residual gravity, expressed in % of g.

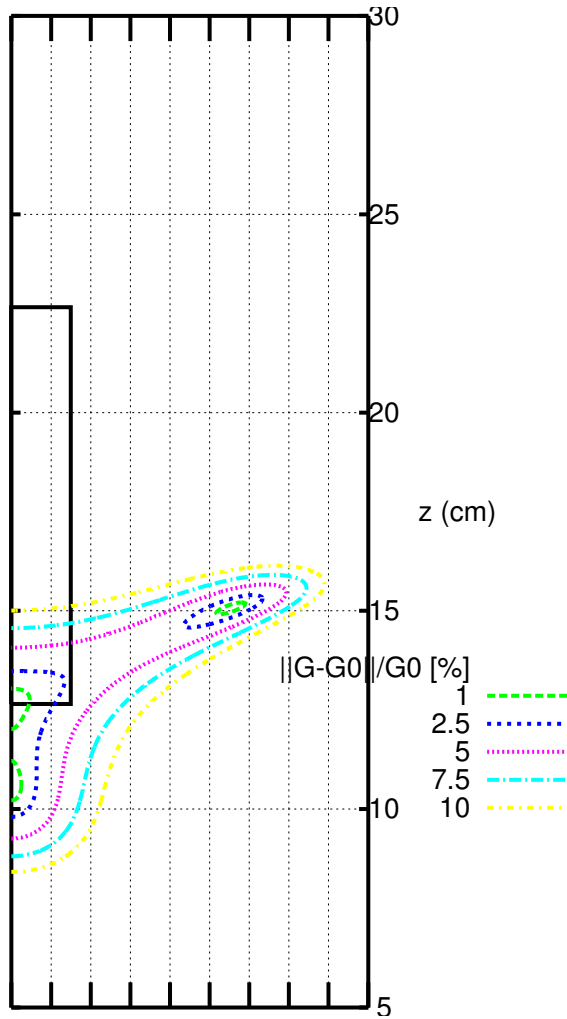


Figure 19: Map of the residual gravity around half a cell

The x-axis scale is 1 cm. Only half of the residual gravity map is presented above, since the second one is symmetric regarding to the coil axis. Half of the cell is represented by the bold rectangle. Its bottom center is placed at the exact compensation point , at 12.6 cm above the center of the coil (0,0)

### 3.2 Sizing of some elements

In cryogenics, everything is sized. There is no place for chance. In this section the sizing of two different elements is presented: the current supply wires and the thermal heat exchanger.

### 3.2.1 Sizing of the current supply wire

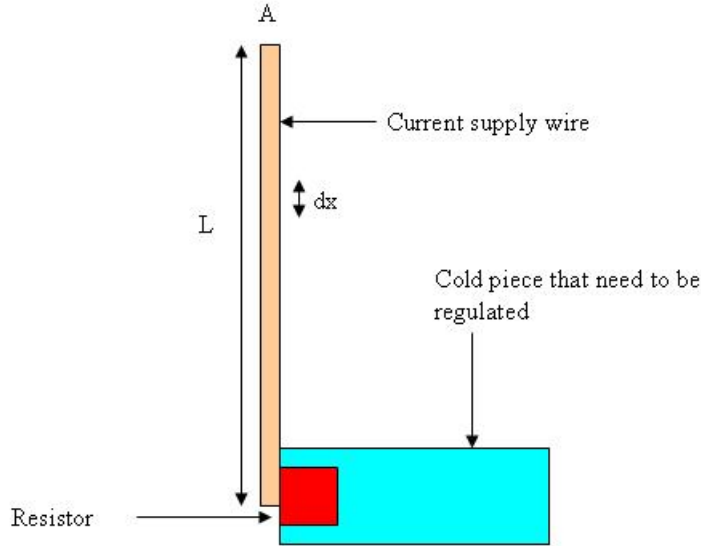


Figure 20: Drawing of the principle element needed to size current supply wire.

Figure 20 presents the main element used to size current supply wire. A one dimension analysis is done.

The power due to joule effect in a wire is

$$dQ = \frac{\rho dx I^2}{A} \quad (22)$$

with  $\rho$  the resistivity in  $\Omega.m$ ,  $dx$  a small length element,  $I$  the current and  $A$  the section of the wire

According to Eq(14), the power due to conduction in the wire is

$$dQ = \lambda A \frac{dT}{dx} \quad (23)$$

with  $\lambda$  the thermal conductivity,  $A$  the section of the wire, and  $T$  the temperature. it leads to :

$$QdQ = \rho \lambda I^2 dT$$

thus:

$$Q^2_f - Q^2_c = 2I^2 \int_{T_f}^{T_c} \rho \lambda dT$$

with  $Q_f$  the power brought at the cold part and  $Q_c$  the power brought at the hot (the other) part of the wire. Moreover,  $Q_f = Q_{cond} + Q_{joules}$  since in vacuum, all power due to joule effect is evacuated by conduction. The goal is to reduce heat input. Hence,  $Q_c = 0$  is imposed due to the thermalisation. Since we are looking for minimizing the heat flux at the cold part, we need  $Q_{cond} = Q_{joule}$ , hence:

$$\frac{A}{L} \int_{T_f}^{T_c} \lambda \, dT = \frac{I}{2} \sqrt{2 \int_{T_f}^{T_c} \rho \lambda \, dT}$$

The Wiedemann-Frantz formula gives  $\lambda \rho = LT$ , with  $\lambda$  the thermal conductivity,  $\rho$  the resistivity  $T$  the temperature and  $L = 2.44 * 10^{-8} W.\Omega.K^{-2}$  a constant. It finally leads to :

$$\frac{LI}{A} = \frac{2 \int_{T_f}^{T_c} \lambda \, dT}{\sqrt{L * (T_c^2 - T_f^2)}} \quad (24)$$

Since a thermalisation is done on a thermal shield at 80 K, the problem is splitted in two part: from ambient temperature at 300K to 80 K and from 80 to 20 K

- For the first case: the needed power to bring is overestimated at 20 W. With a resistor of 100  $\Omega$ , it corresponds to  $I=0.44A$ . Tables give the conductivity integral between 300K and 80K : 76625,48  $W.m^{-1}$ . Hence, we get :  $b = \frac{LI}{A} = 3.5 * 10^{-4} A/cm$  . The length of the wire  $L'$  is 3m, then its diameter is :

$$\Phi = \sqrt{\frac{AL'I}{\pi b}}$$

$$\Phi = 0.7mm$$

- The same reasoning gives a diameter of 0.2 mm between 80 and 20 K, where the length of the wire is 50 cm.

### 3.2.2 Sizing of the thermal shield heat exchanger

A thermal shield is placed all around the cell in order to reduce the radiative heat coming from the hot (300K) vacuum vessel of the cryostat.

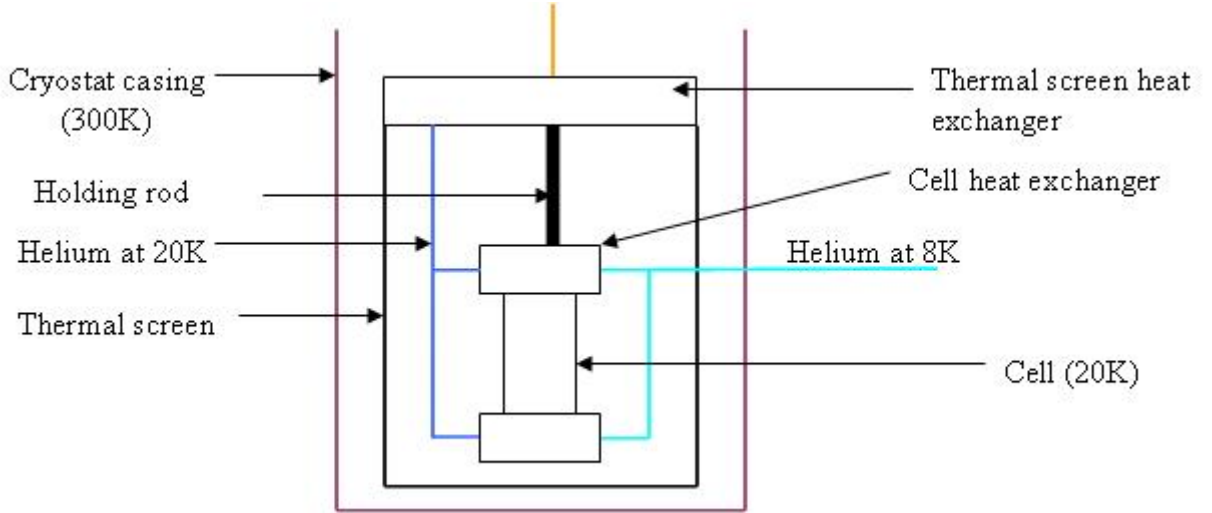


Figure 21: Drawing of the principle elements in the vicinity of the thermal shield.

As shown in figure 21, cold gas helium, coming from a tank ( not drawn on the right side of the figure), arrives into the cell to cool it down. Because of the heat exchanger pipe length, the helium temperature at the cell outlet is 20K. The helium gas is then utilized to cool down the thermal shield. In the following, one shows how this shield is size up.

Moreover, an additional power of 2W is set on the cell during the experiment, to control the temperature very precisely.

- Calculation of the needed flow rate

Firstly, the thermal shield exchanger is considered as perfect : the temperature of the shield is equal to the temperature of the leaving helium.

The heat balance of the cell has to be done : it receive radiating power from the thermal shield, the 2W additional power and the conduction power coming from the handling rod.:

$$\Phi_1 = F_{1 \rightarrow 2} \sigma \epsilon S (T_{screen}^4 - T_{cell}^4) + 2W + P_{cond}$$

with  $\sigma$  the Stephan constant,  $\epsilon$  the emissivity and S the area of the cell. For long cylinders,  $F_{1 \rightarrow 2}$  is equal to:

$$F_{1 \rightarrow 2} = \frac{\epsilon_1 \epsilon_2}{\epsilon_2 + \frac{A_2}{A_1} (1 - \epsilon_2) \epsilon_1}$$

For small emissivity, such as in our case (between 0.02 and 0.1 for copper and between 0.1 and 0.2 for steel),  $F_{1 \rightarrow 2}$  is often approximated by  $F_{1 \rightarrow 2} \approx 0.5$ . As this heat is evacuated with the heat exchanger, one gets :

$$\Phi_2 = m' C_p (T_{of} - T_{if})$$

with  $m'$  the helium flow rate,  $T_{of}$  the temperature of the leaving helium,  $T_{if}$  the temperature of the incoming helium and  $C_p$  the thermal capacity (in J/kg/K).

Then, the heat balance of the thermal shield has to be done: it receives radiative power from the cryostat vacuum vessel.

$$\Phi_3 = F_{1 \rightarrow 2} \sigma \epsilon S (T_{casing}^4 - T_{screen}^4)$$

In our case, the previous relation becomes

$$\Phi_3 = 0.5 \sigma \epsilon S (T_{casing}^4 - T_{screen}^4)$$

and evacuates it with its heat exchanger and by conduction into the handling rod:

$$\Phi_4 = m' C_p (T_{ots} - T_{of}) + P_{cond}$$

with  $T_{ots}$  the temperature of the leaving helium.

$P_{cond}$  is calculated according to Eq(14). The values of the integral of conductivity, coming from tables has been linearised.

Calculations have been done using an iterative method: first, the flowrate is chosen and imposed. Using  $\phi_1 = \phi_2$  the temperature of the thermal shield is calculated.

This value is then put into the equation  $\phi_3 = \phi_4$ . A new value of the flowrate is then obtained. This loop is done until reaching convergence. The final flowrate is 745 L/H of helium gas at normal temperature and pressure.

- Calculation of the thermal shield exchanger temperature

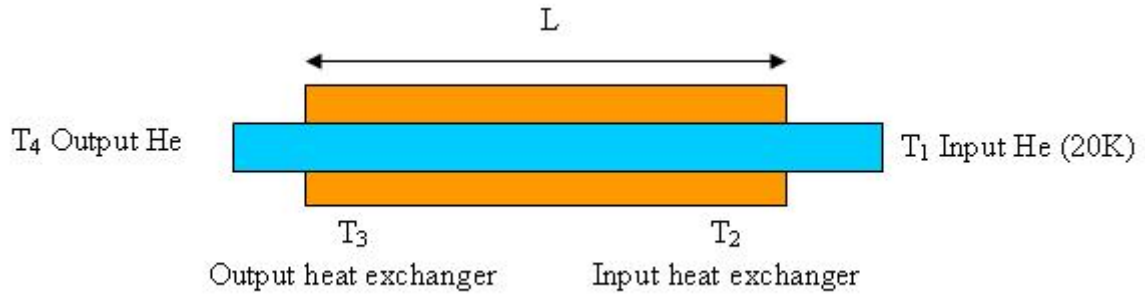


Figure 22: Drawing of the thermal shield exchanger: the core (in orange) and the pipe (in blue).

The exchanged power is given by :

$$\phi_5 = hS\Delta T_{log}$$

with h the convection coefficient, S the exchange area and

$$\Delta T_{log} = \frac{(T_2 - T_1) - (T_3 - T_4)}{\ln\left(\frac{T_2 - T_1}{T_3 - T_4}\right)}$$

This power is also equal to

$$\phi_5 = m'C_p(T_4 - T_1)$$

As same as previously, the method is iterative. The following system has to be solved:

$$\phi_5 = \phi_6 = \phi_3 - P_{cond}$$

By imposing a length of 359 mm, and the flowrate previously obtained, it corresponds to a final temperature of the thermal shield of **60K**, using  $\epsilon = 0.1$  for the copper emissivity

### 3.3 Experimental protocol

After having described the installation, its surrounding and the sizing of some element, let's enter into the experimental part. A protocol is established to cool the installation down. It is described in the following chapter.

### 3.3.1 Starting the installation

In this section, the protocol to prepare, run and stop an experiment of boiling crisis of liquid hydrogen in magnetic levitation is described. To understand this protocol, it is necessary to refer to different parts below on figure 23.

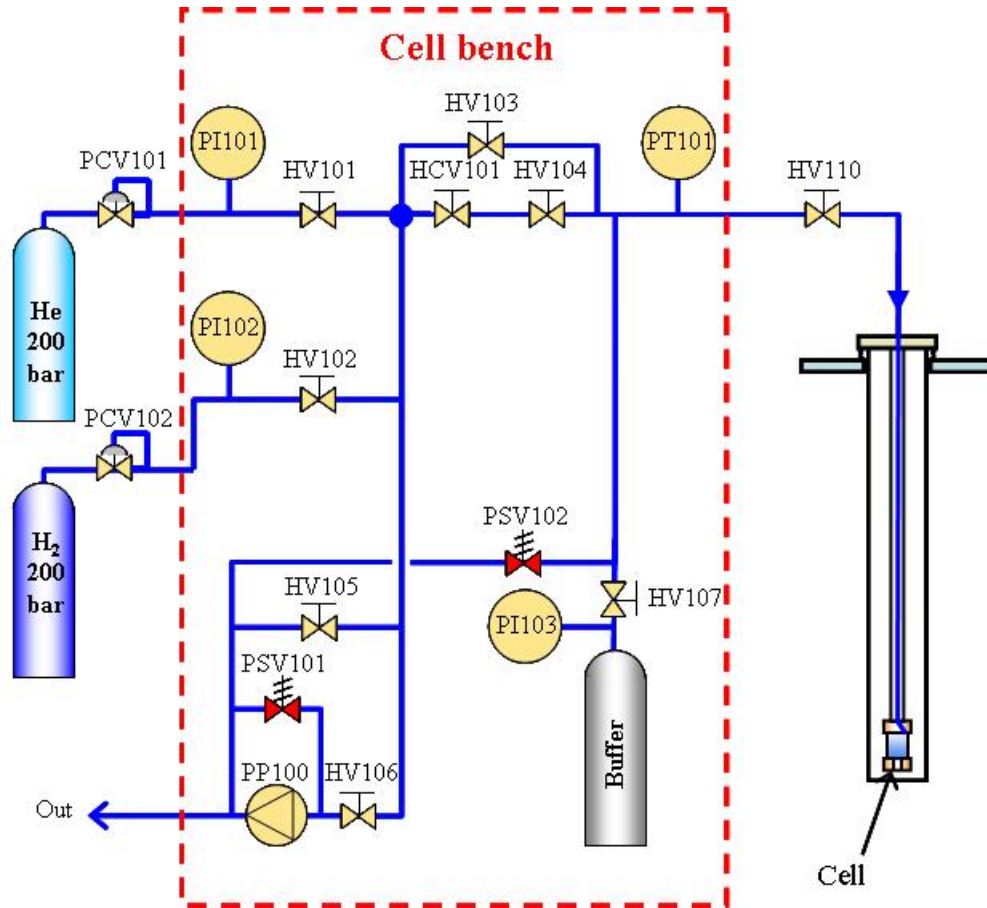


Figure 23: Drawing of the fluid feeding system of the cell.

The experimental protocol consists of the following steps:

**Simple checks:** A number of checks are performed before all things:

- Test all heaters, thermometers, flow meters and pumps of the cryostat.

### **Installation of the experimental cells:**

Before inserting the cell in the cryostat:

- Check the good behaviour of thermometers and heating of the cell,
- Check for any possible leaks of hydrogen and helium circuit of the cell by applying a vacuum in both circuits, then doing a leak detection with helium. The leakage rate must be less than  $10^{-8}mb.l/s$ . Let the circuit at atmospheric pressure after the test.

### **Installation of the cryostat inside the coil:**

The cryostat is inserted into the field hole of the coil with the overhead crane. This operation is very delicate. It is performed using the crane available in the hall of LNCMI. Since the cryostat is very high, movements of the crane can generate an important deviation. The introduction of the cryostat must be very slow in order to keep everything safe inside.

### **Vacuum in the cryostat:**

When the cryostat is placed in the hole, a secondary vacuum has to be proceeded, by connecting a pump to the valve PV100 (see figure 13). The vacuum in the cryostat must be of the order of  $10^{-5}$  mbar. The pressure gauge is given by the PT102.

### **Rinsing and draining of the experimental cell:**

it is a necessity to purge the experimental cell under helium as follows:

- Starting of the pump PP100 (pumping of the cell),
- Opening the valves HV106 and HV103. Valves HV101, HV102, HV104 and HV105 are closed. The valve HV110 must always remain open,
- When the pressure is low enough ( $PT101 = 10^{-1}mb$ ), the manual valve is operated closed HV106,
- Opening of the helium bottle and valve HV101 until a pressure of 2 bar on PT101,
- Closing of the valve HV101,
- Repeat these steps 3 times.

The cell must remain under helium. HV101 valve must remain open. The helium pressure is 2 bars.

### Cooling and filling of the cell:

- Connection of the helium siphon on the helium cooling circuit of the cell.
- Regulation of the helium flow in the two exchangers of the cell to lower its temperature to approximately 20K. The average cooling speed is 150 K/H. The cell is then filled as follows:
  - Closing of HV101 (HV103, HV106, HV107 and HV110 open, HV102, HV104 and 105 closed HV),
  - Pumping the cell with the pump PP100,
  - Regulation of W101 on TT101 to get a temperature of 20K,
  - Regulation of W102 on TT102 to get a temperature of 20K,
  - Regulation of W103 on TT103 to get a temperature of 20K,
  - Closing of the valve PV100,
  - Opening of the bottle of hydrogen,
  - Opening of HV102 slowly so as to fill the cell with liquid hydrogen,
  - Adjustment to the desired pressure when the cell is full, .

Endoscopes must be set, centered on the cell.

### **3.3.2 Stopping the installation**

This last section is devoted to stopping the installation safely. The order of actions is crucial:

- Closing of the valve HV102
- Closing of the bottle of hydrogen.
- Closing of HV100 and cut the flow of helium (FT201 and 202)
- Pumping the hydrogen of the cell,
- Stopping the regulations W101, W102, W103, W201 and W202
- Putting the cell under helium after rinsing of the cell (see previous "Rinse and drain the experimental cell"),
- Closing of the valve HV101

PS100 is a turbo-molecular pump, enabling to have a high secondary vacuum. It's connected in serial with a primary pump. PS100 is very sensitive to magnetic field. Indeed, the rotor of the pump rotates at 36 000 RPM, which could create high eddy current leading to its destruction. That's why it has been placed 6 meters away from the hole magnetic field. However, it creates much more pressure losses in the pumping pipes due to their length. Hence the pumping of the cryostat is much slower. In this experiment it's a dynamic vacuum: the pump is always running, even when the installation is hot (300K). Thus the pumping time is no longer a problem.

### 3.3.3 Running of a measurement campaign

After all these descriptions, it could be interesting here for the reader to remember the main objective of this campaign: the establishment of the Nukiyama curve for Liquid hydrogen ( $LH_2$ ), (see figure 8) in microgravity.

#### Finding of the exact compensation point:

For experiments at normal gravity, as soon as the cell is at 20K, measurements can start. However, for microgravity of 0g and 0.1g, the exact compensation point has to be found. First of all, the cryostat is moved vertically by a lift table to place the cell at its theoretical position determined by the magnetic map (see figure 19). The current in the coil is risen until reaching its theoretical value.

A small heat flux density is then applied to create some bubbles. Figure 6 explained why hydrogen is radially unstable. Hence, at 0g, bubbles should move radially. The observation of phenomenon is done directly by using the camera.

If bubbles are still going up, the current is increased until getting the radial boiling. The speed of the bubble is also a precious information to find the compensation point: indeed, the closer to this point, the slower the bubbles. A scanning of a large band of current is done all around the point to be sure of having the real compensation point.

In our case, this point was obtained for a current of 25100 A in the inner coil and 20541 A in the outer one, corresponding to a magnetic field of 14.31 T at the magnetic center. The description of these coils is precisely done in Appendix section.

The boiling curve is obtained by applying an heat flux density. it can be useful to remind that the overheating is defined by

$$\Delta T_{sat} = T_{wall} - T_{sat}$$

When the heat flux is imposed for the first time, the overheating can be very high before getting boiling: several nucleation sites can stay inactive. To activate all of them, a quite high flux, to the order of magnitude of the critical heat flux (CHF) is imposed. Measures can then start and are totally reproducible for a same heat flux. The temperature of the wall is measured by the thermal sensor TT100 (see its position

in figure 18 page 29), and the heat flux is imposed directly across the resistance. this power is entirely transmitted to the liquid.

Whatever the gravity, measures and the detection of the CHF remain the same: it's a thermal manner.

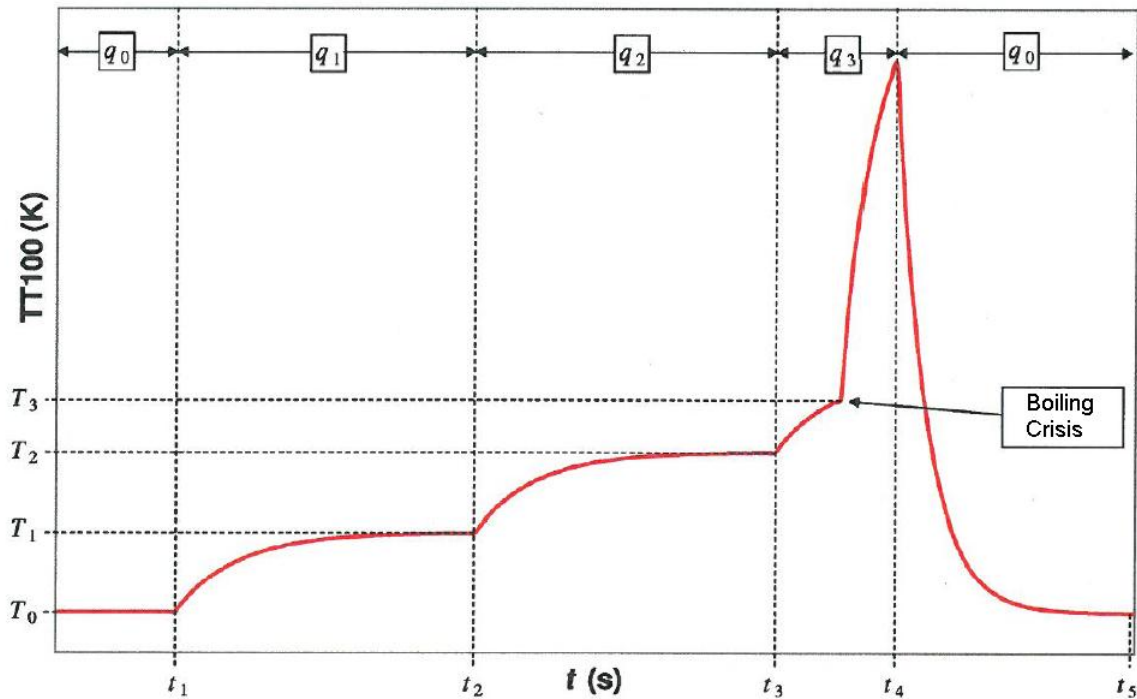


Figure 24: Time evolution of the heating element (TT100) during the detection of CHF

As shown on figure 24, the brutal increase of the temperature for an almost constant flux is characteristic of the CHF.

As soon as the CHF is detected, the imposed flux is reduced to prevent the heating element to be destroyed.

**Procedure:**

This description will be done using figure 24.

Let's call  $T_0$  a minimum temperature, smaller than the minimal temperature corresponding to the flux of film boiling mode. The heating compound is maintained to this temperature by applying a flux  $q_0$ .

At the time  $t_1$ , the flux is increased to  $q_1$ . the temperature evolves. At  $t \lesssim t_2$ , when the temperature is stable( $TT100=T_1$ ), the point is taken.

At the time  $t_2$ , the flux is increased to  $q_2$ . the temperature evolves. At  $t \lesssim t_2$ ,

when the temperature is stable( $T_{100}=T_2$ ), the point is taken.

At the time  $t_3$ , the flux is increased to  $q_3$ . after a short time, the temperature increases rapidly: it's the boiling crisis.  $T_3$  is a value close to the maximum overheating. Hence, the critical flux is between :

$$q_2 < q_{CHF} < q_3 \quad (25)$$

the flux is then decreased to the first value. This procedure is then reproduced using a smaller value  $q'_3$  instead of  $q_3$ .

If the boiling crisis appears, then is obvious that

$$q_2 < q_{CHF} < q'_3 \quad (26)$$

Otherwise,

$$q'_3 < q_{CHF} < q_3 \quad (27)$$

The precision criterion has been chosen at 0.5W on the flux.

## 4 Results

This master thesis has been done in collaboration with CEA Grenoble, LNCMI, Air liquide and CNES (the french Space Agency). Several measurements have been imposed during experimental campaign, defined in a contract. There was a confidentiality clause in this contract, that's why the curves are presented here without any scale on their axis, in order to keep confidentiality.

Several Boiling curves had to be established for different thermodynamics properties that are presented on the following table:

Level of gravity	Pressure (bar)	Temperature (K)
1 g	1	$T_{sat} = 20.23$
	1	$T_{sat} - 2 = 18.23$
	2	$T_{sat} - 0.5 = 22.33$
	2	$T_{sat} - 2 = 20.83$
0 g	1	$T_{sat} - 2 = 18.23$
	2	$T_{sat} - 2 = 20.83$
0.1 g	1	$T_{sat} - 2 = 18.23$
	2	$T_{sat} - 2 = 20.83$

Table 1: Resume of the measurements that have to be performed

## 4.1 At 1g

### 4.1.1 1bar at saturation

The first curve has been done for 1 bar and the corresponding saturation temperature.

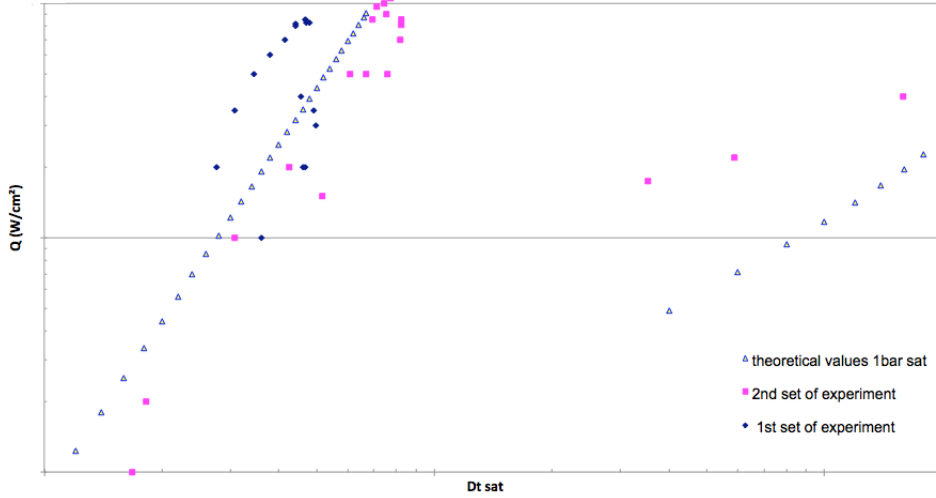


Figure 25: Nukiyama's curve of liquid hydrogen at 1bar and the corresponding saturated temperature under 1g.

The cell was half empty to be sure that the saturation condition were fulfilled. The pool boiling part of theoretical curve corresponds to Kutelatdze correlation [2]:

$$q = 1.8 * 10^{-13} \frac{k C_p^{1.5} \rho_l^{1.28} p^{1.75}}{\mu^{0.625} \sigma^{0.9} \lambda^{1.5} \rho_v^{1.5}} \Delta T_{sat}^{2.5} \quad (28)$$

Where  $q$  is the heat flux (in  $W.cm^{-2}$ ),  $k$  is the thermal conductivity (in  $W.m^{-2}.K^{-1}$ ),  $C_p$  is the specific heat capacity (in  $J.kg^{-1}.K^{-1}$ ),  $\rho_l$  is the density of the liquid,  $p$  is the pressure (in Pa),  $\mu$  is the viscosity in Pa.s,  $\sigma$  is the surface tension (in N/m),  $\lambda$  is the latent heat of vaporisation (in J/kg) and  $\rho_v$  is the density of the vapour.

The film boiling part of the theoretical curve corresponds to Breen and Westwater correlation [2]:

$$q = \frac{0.37 + 0.28 \left( \frac{\sigma}{g D^2 \Delta \rho_f} \right)^{1/2}}{\left( \frac{\sigma}{g \Delta \rho_f} \right)^{1/8} \left( \frac{\mu_f \Delta T}{k_f^3 \rho_f g \lambda'} \right)^{1/4}} \Delta T \quad (29)$$

Where  $D$  is the characteristic length (in m). For this correlation,  $\lambda'$  is the effective heat of vaporization given by [2]:

$$\lambda' = \frac{(\lambda + 0.340 C_p \Delta T)^2}{\lambda} \quad (30)$$

There have been two different sets of experiments which gave quite dispersive results.

The cell has then be totally filled with liquid hydrogen. It enabled to impose a smaller temperature than the saturated one for a fixed pressure. Moreover, the temperature of the liquid pool is ever better controlled since both exchangers are in contact with the liquid.

#### 4.1.2 1bar and $T=T_{sat}-2K$

The following curve has been done with a temperature 2K smaller than the saturated one for 1bar :  $T=18.23K$

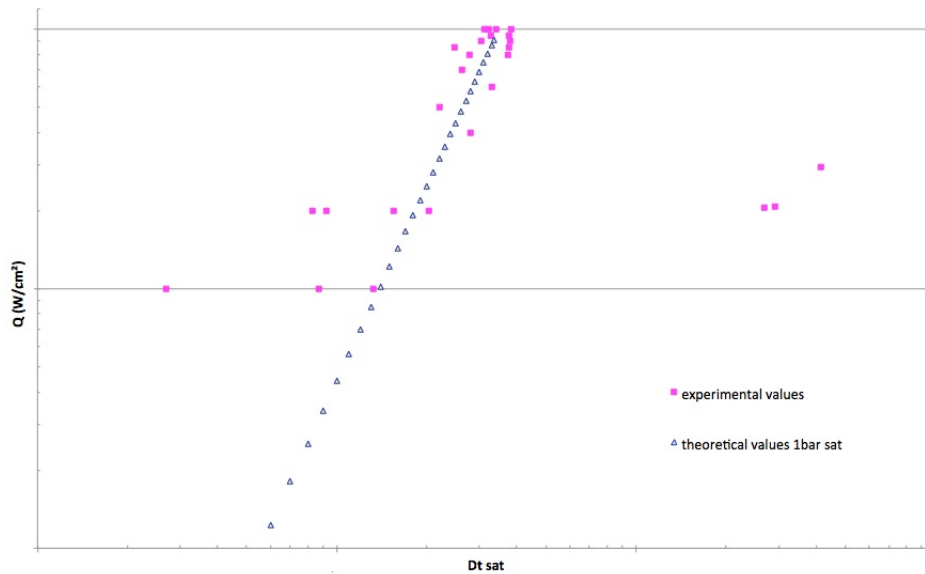


Figure 26: Nukiyama's curve of liquid hydrogen at 1bar and  $T_{sat}-2K$  under 1g.

As shown in figure 26 above, results are closer one from each other and also close to the theoretical curve. However it can be underlined that this theoretical one is the same as the previous one. Indeed, as it can be seen on Eq (28), since for liquid hydrogen, the influence of the temperature is very small on different paramater (such as  $C_p$ , etc...), the subcooling of this liquid is neglectible on the shape of the curve.

There are some points for small overheating which are suspicious. They have been done at the very end of this set of experiment. Before emptying the cell, some small impurities have been seen at its bottom. It could have been some oxygen or nitrogen ice-cube present due to a small leak in the hydrogen feeding system. These impurities could be the reason of these last measurements.

Then all the circuit has been controlled and all manual valves have been verified and tightened before starting the next set of experiments.

### 4.1.3 2 bars and $T = T_{sat} - 0.5K$

The pressure has then be increased to 2 bars and the temperature has been regulated to  $T = T_{sat} - 0.5 = 22.33K$ . Results are shown below:

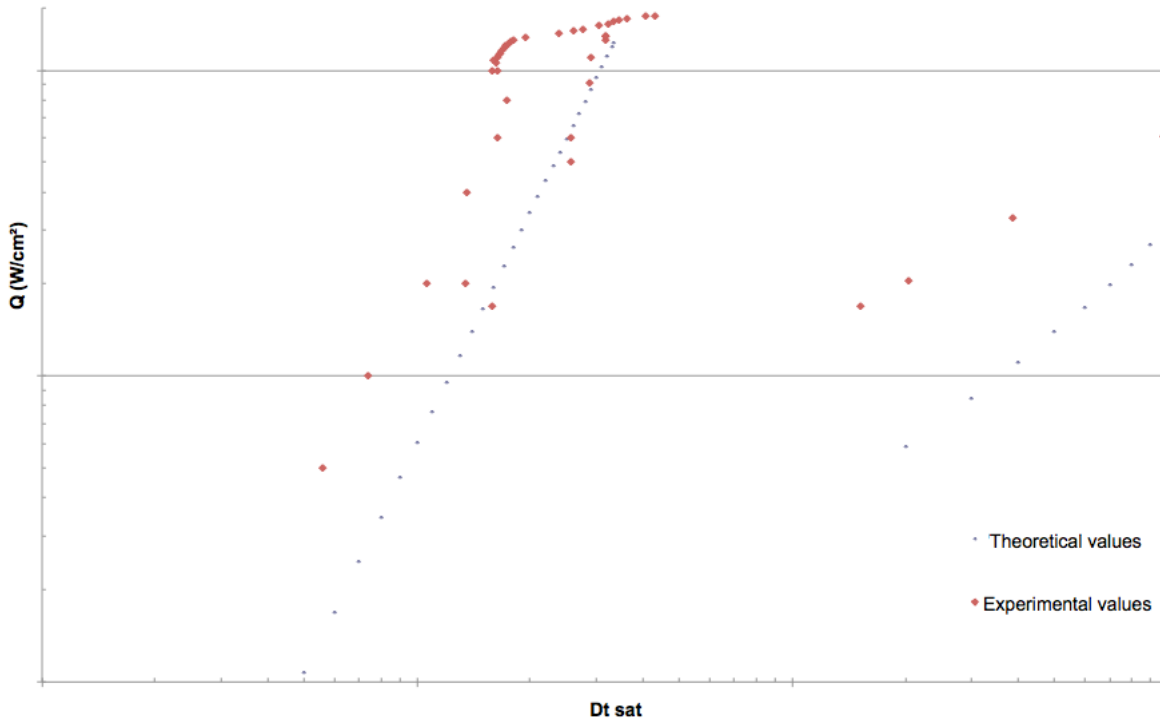


Figure 27: Nukiyama's curve of liquid hydrogen at 2bar and  $T_{sat} - 0.5K$  under 1g.

The theoretical curve has been established thanks to eq (28), with the data extracted from NIST table.

As it can be seen in figure 27 the experimental value of the CHF is much higher than the theoretical one. This measurements are also in general shifted to the left, i.e the overheating is smaller, the heat transfer is better.

#### 4.1.4 2 bars and $T = T_{sat}-2K$

The temperature has then be decreased to  $T = T_{sat}-2=20.83K$  , keeping the same pressure. Results are shown below:

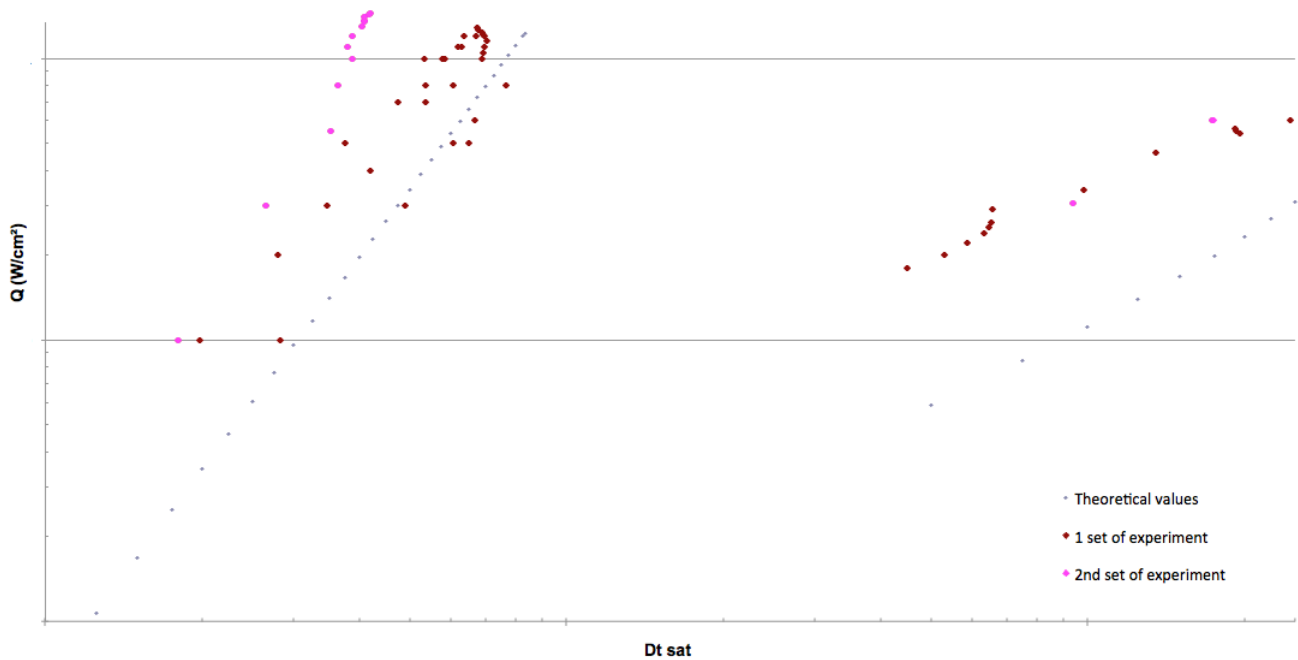


Figure 28: Nukiyama's curve of liquid hydrogen at 2bar and  $T_{sat}-2K$  under 1g.

As shown in figure 28, two sets of experiment have been carried out. Whereas both of them are similar in the film boiling part, in the nucleate boiling one, there are some discrepancies. These two sets have been done one day apart.

In the second one the thermal transfer was much better since the overheating is shifted to the left. Moreover it can be seen that the CHF was found higher in the second one than in the first one, which is coherent with the previous affirmation. Indeed, the better the heat transfer, the higher the CHF.

## 4.2 At 0g

The magnetic field has then been set to obtain the microgravity conditions (see figure 19 page 31). The exact compensation point of the gravity has been found experimentally by fixing the correct height and progressively increasing the current in the coil, i.e. increasing the magnetic field. The evolution of the shape of bubble are observed using the camera.

As soon as bubbles grow radially and very slowly, the couple  $(I, z)$  is defined as the right one. Measurements can then start and results are shown in the following figures

### 4.2.1 1 bar and $T = T_{sat} - 2K$

The first set of measurements has been done for a pressure of 1 bar and a temperature 2K smaller than its saturated one:  $T = 18.23K$ .

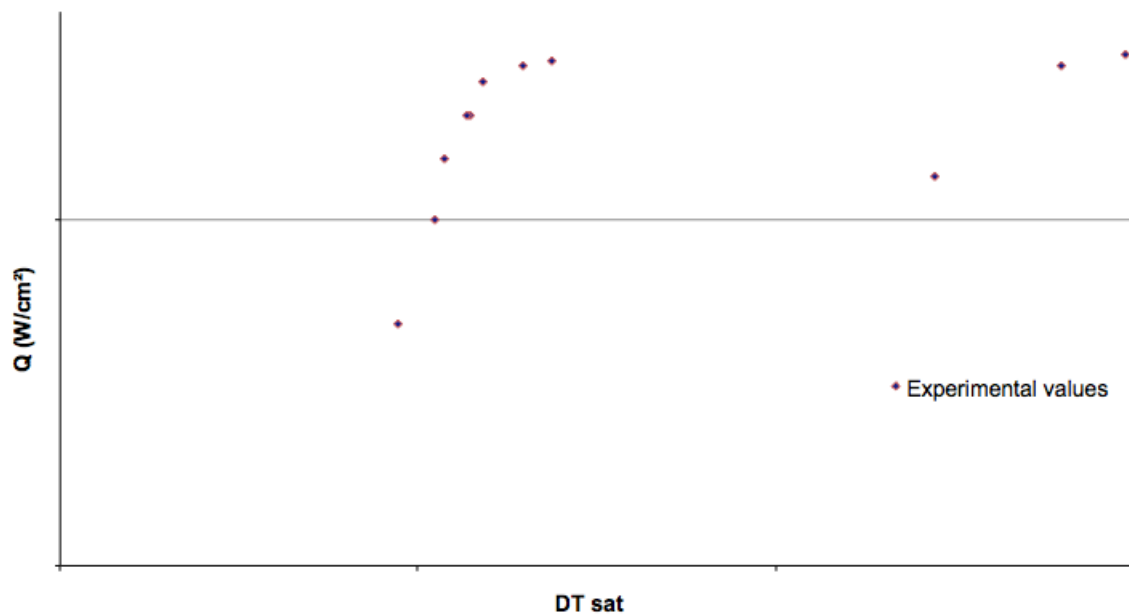


Figure 29: Nukiyama's curve of liquid hydrogen at 1bar and  $T_{sat} - 2K$  under 0g.

The reproducibility of the results has been well obtained. Indeed as it can be seen in figure 29, for the same imposed heat flux, the overheating is almost exactly the same.

The shape is as expected. However, even if in this master thesis no values can be expressed, it can be notified that the CHF is very different from the same configuration under normal gravity (1g).

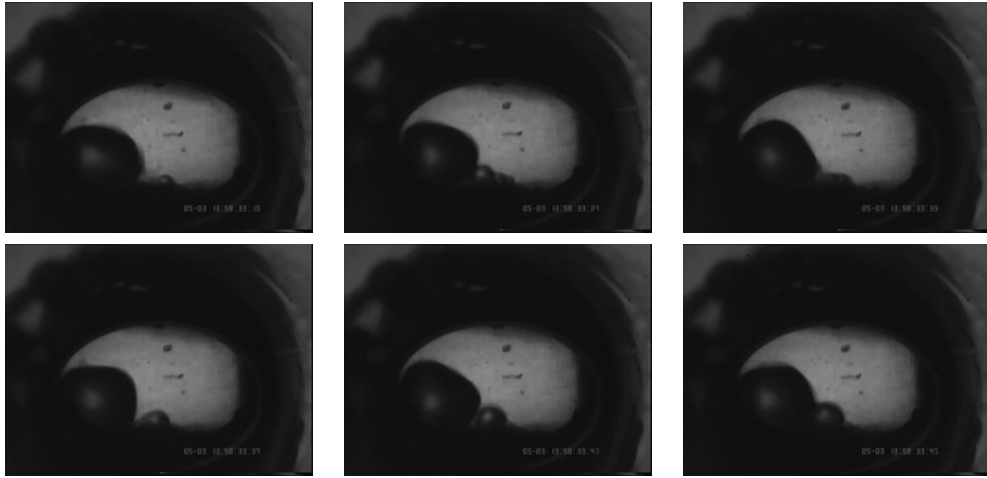


Figure 30: Snapshots of the video of nucleate boiling under 0g at 1bar and  $T_{sat}-2K$ , from upper left corner to downner right one

As it can be seen above, under 0g, bubble are leaving radially the heater, to agglomerate on a bigger bubble at one side of the cell.

figure 30 shows the film boiling in 0g for these thermodynamic conditions:

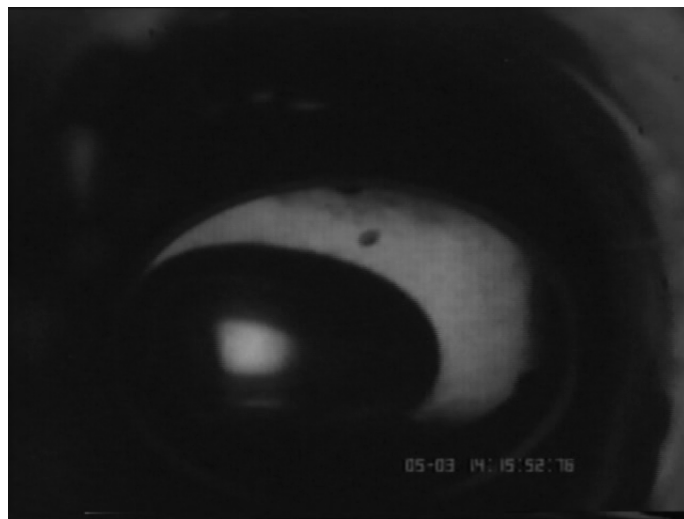


Figure 31: Snapshots of the video of nucleate boiling under 0g at 1bar and  $T_{sat}-2K$

As expected, the bubble is immobile. All the evaporated liquid is condensed at the interface. This big bubble is almost 10mm high and 20mm long.

#### 4.2.2 2 bars and $T = T_{sat} - 2K$

The pressure is then up to 2 bars and the temperature is regulated to  $T = T_{sat} - 2 = 20.83K$ . The following figure shows results.

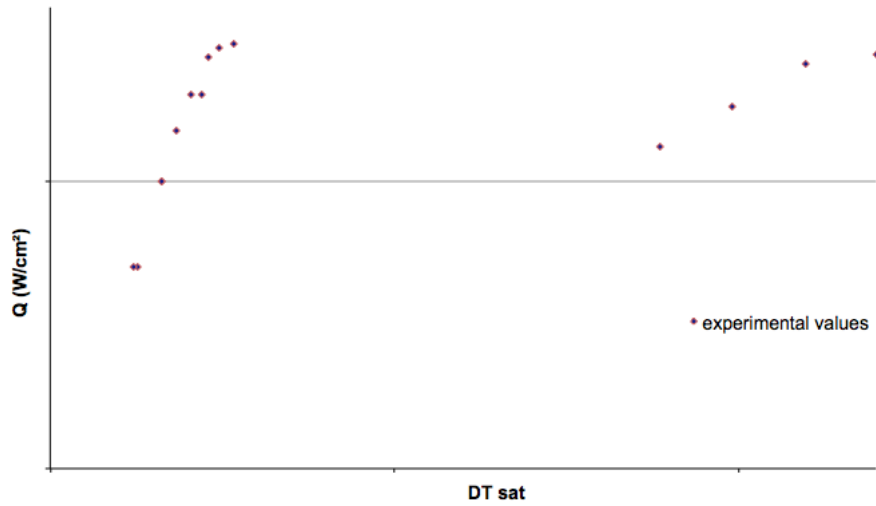


Figure 32: Nukiyama's curve of liquid hydrogen at 2bar and  $T_{sat} - 2K$  under 0g.

In figure 32, it can be seen that here also the reproducibility is good. Which enable to assert that everything is correct. Moreover, the expected shape is also obtained.

## 4.3 Under 0.1g

### 4.3.1 2 bars and $T=T_{sat}-2K$

To obtain 0.1g, the current is calculated according to Eq (13), page 11. It led to an intensity of 23812 A in the inner coil and 19487 A in the outer coil. The resulting magnetic field at the center of both coils is 13.58 T.

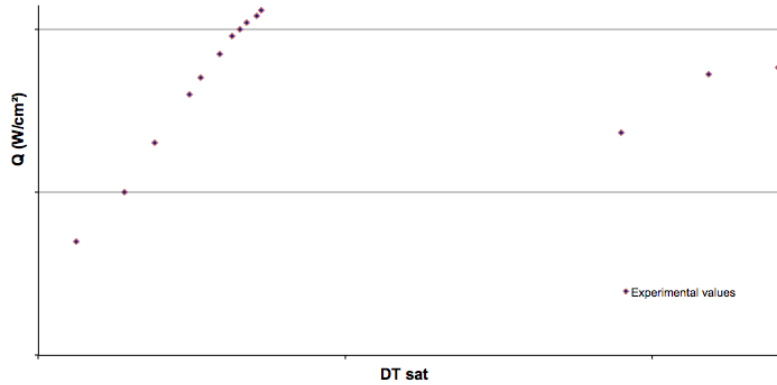


Figure 33: Nukiyama's curve of liquid hydrogen at 2bar and  $T_{sat}-2K$  under 0.1g.

Obtained results are very satisfying, and the reproducibility is also been verified. The global shape fits totally as expected.

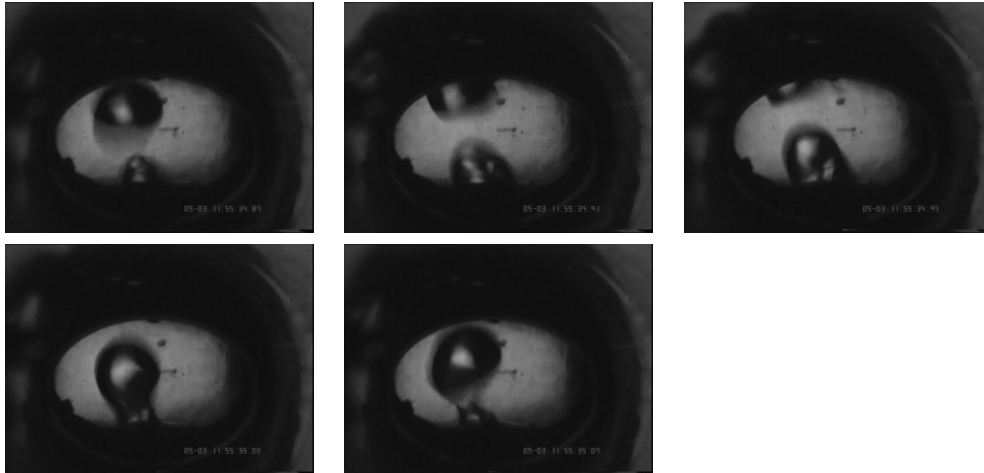


Figure 34: Snapshots of the video of film boiling under 0.1g at 2bar and  $T_{sat}-2K$

In the first picture (upper left corner), the big leaving bubble can be seen and another one is forming. The size of the bubbles explicitly shows that we are in film boiling. Indeed, the bubble measure around 13 mm diameter ; which is higher than the heating compound size. The power injected by the heater is 4.9W

## 5 Discussion

In the previous section, row have to be carried out to obtain real values for the heat flux and the measured temperature.

### 5.1 Corrections

#### 5.1.1 Temperature of the heating part

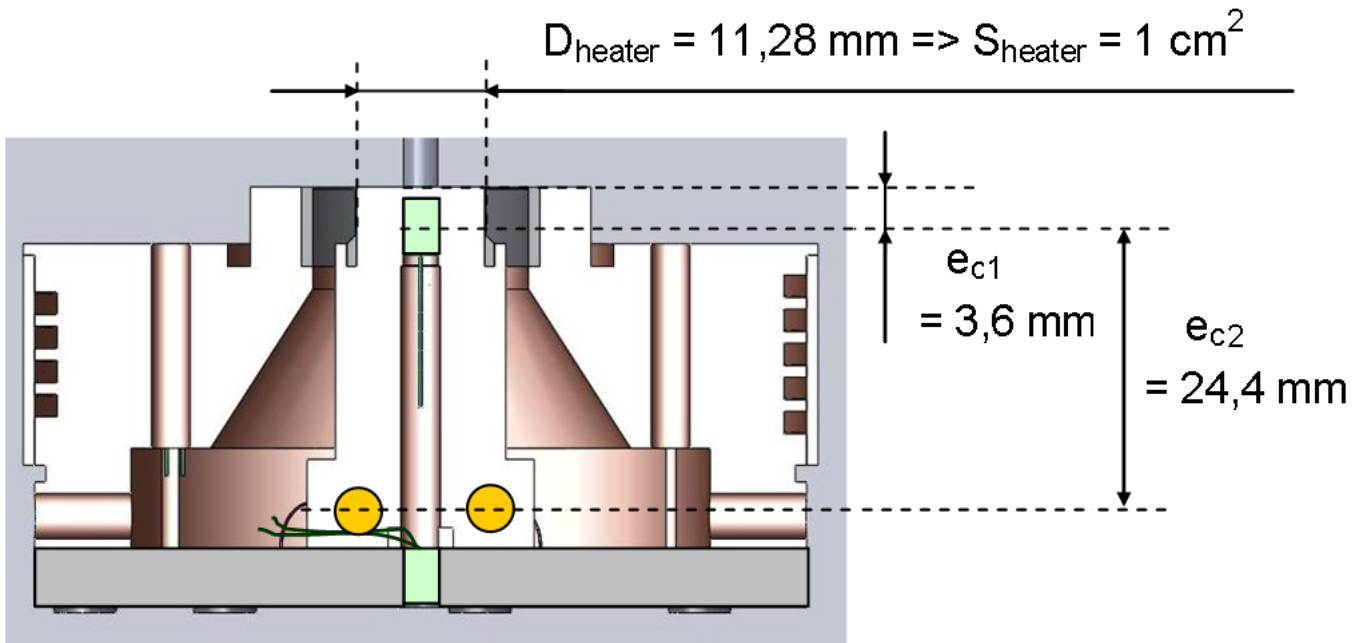


Figure 35: Position of the thermal sensor in the heating compound (green rectangle on the top).

The real temperature of the heater is given by:

$$\Delta T_{real} = T_{meas} - \Delta T_{cond}$$

$$\text{with } \Delta T_{cond} = \frac{4P_{meas}e_{c1}}{\lambda_c \pi D_{heater}}, \text{ and } P_{meas} = UI$$

All values are in SI units. Here  $e_{c1} = 3.6 * 10^{-3}m$ ,  $\lambda_c = f(T_{meas})$  and  $D_{heater} = 1.128 * 10^{-2} m$ .  $\Delta T_{real}$  is the real temperature of the wall (in K).  $T_{meas}$  is the measured temperature of the sensor,  $\Delta T_{cond}$  is the temperature difference between the sensor and the wall,  $P_{meas}$  is the imposed power (in W),  $e_{c1}$  is the distance between the sensor and the wall,  $D_{heater}$  is the diameter of the heating compound.

This is the main correction that has to be applied to obtain true values for the wall temperature of the heating area.

### 5.1.2 Pressure in the cell

The real pressure in the cell is given by :

$$P_{real} = P_{meas} + \Delta P, \text{ with } \Delta P = \rho_{H_2} \cdot A \cdot g \cdot h$$

Where  $\rho_{H_2} = 70.3 \text{ kg/m}^3$  at 1 bar and 20K, A is the percentage of g (0%, 10% or 100%), and h is the height of the cell (0.1m).

The estimation of the height of the liquid hydrogen corresponds to the height of the sapphire tube, added with the height of the upper bridle. During experiment, this height can be higher. Hence, this correction  $\Delta P$  is the minimum one to apply to measured pressures  $P_{meas}$ . Corrections  $\Delta P$  are respectively 0.69, 0.069 and 0 mbar for 1g, 0.1g and 0g.

### 5.1.3 Power transfered to the liquid

The real power transfered to the liquid via the heating area is (see figures 35 and 36

$$P_{real} = P_{meas} - W_1 - W_2 - W_3 \quad (31)$$

Where  $W_1$  (in W) is the losses in the titanium ring,  $W_2$  (in W) is the losses in the disc and  $W_3$  is the losses in the current supply wires.

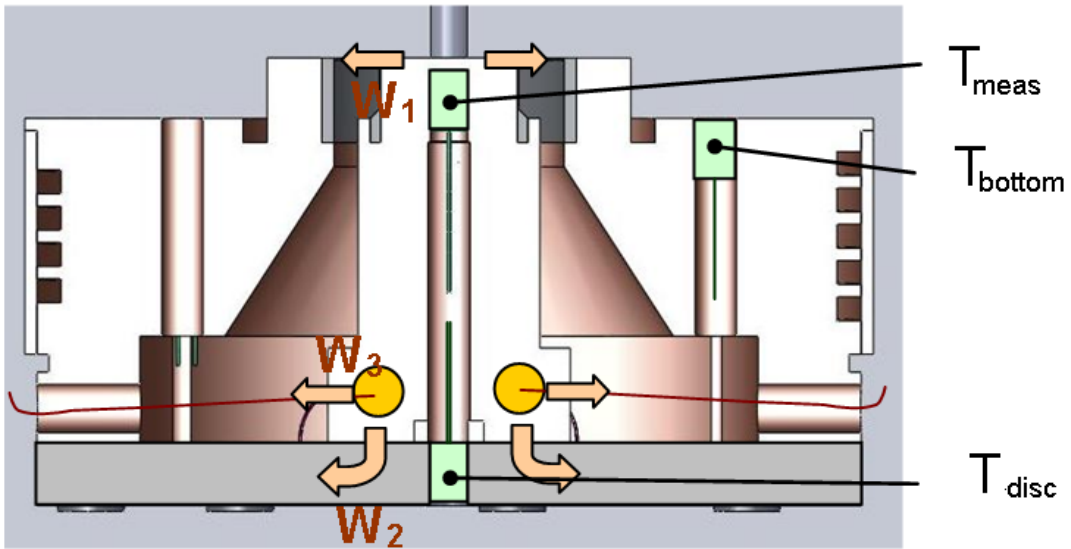


Figure 36: description of the different powers taking place in the heating compound.

$$W_1 = \frac{2\lambda_{tit}\pi e_{ring}(T_{real} - T_{bottom})}{\ln\left(\frac{R_{ring}}{r_{ring}}\right)} \quad (32)$$

Where  $\lambda_{tit} = f\left(\frac{T_{real} - T_{bottom}}{2}\right)$ ,  $e_{ring} = 0.1 * 10^{-3}$  m,  $R_{ring} = 9.5 * 10^{-3}$  m and  $r_{ring} = 5.74 * 10^{-3}$  m.

$$W_2 = \frac{2\lambda_{G10}\pi e_{disc}(T_{disc} - T_{bottom})}{\ln\left(\frac{R_{disc}}{r_{disc}}\right)} \quad (33)$$

Where  $\lambda_{G10} = f\left(\frac{T_{disc} - T_{bottom}}{2}\right)$ ,  $e_{disc} = 5 * 10^{-3}$  m,  $R_{ring} = 3.4 * 10^{-2}$  m and  $r_{ring} = 1.55 * 10^{-3}$  m.

$$W_3 = \frac{\lambda_c \pi d_{wire}^2 (T_{real} + \frac{e_{c1}}{e_{c2}} \Delta T_{cond} - T_{therm})}{4l_{wire}} n_{wire} \quad (34)$$

Where  $n_{wire} = 2$ ,  $l_{wire} = 0.5$  m, and  $d_{wire} = 2 * 10^{-4}$  m, and

$$\lambda_c = f\left(T_{real} + \frac{e_{c1}}{e_{c2}} \Delta T_{cond} - T_{therm}\right)$$

It corresponds to the following maximal errors:

Nucleate boiling	Film boiling
$W_{1max} = 2.3\% P_{meas}$	$W_{1max} = 10.4\% P_{meas}$
$W_{2max} = 1.3\% P_{meas}$	$W_{2max} = 1.05\% P_{meas}$
$W_{3max} = 0.2\% P_{meas}$	$W_{3max} = 0.4\% P_{meas}$

Table 2: Errors related to the measured power  $P_{meas}$

## 5.2 Uncertainties on the losses related to the titanium ring

Measurements of these uncertainties have been done while the cell was under vacuum. The temperature difference between each side of the ring ( $\Delta T$ ) is plotted as a function of the power. Figure 37 shows the difference between the theoretical curve and the obtained measurements.

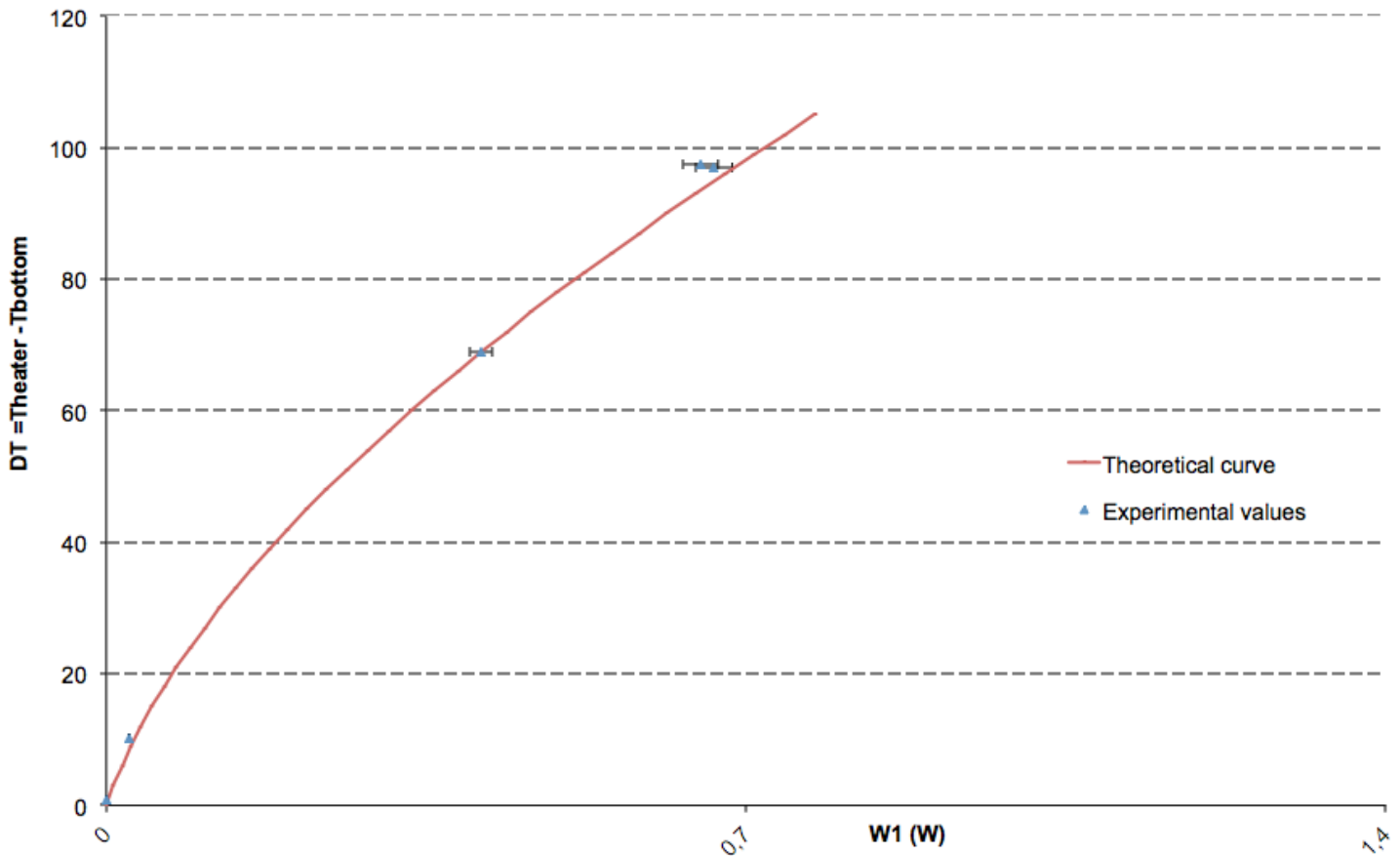


Figure 37: Radial losses in the titanium ring

The maximum deviation from the theoretical curve correspond to 3% of the measured value, which is totally acceptable.

## 5.3 Comparisons

### 5.3.1 Effect of the gravity

In the following condition of pressure and temperature, when the gravity level increases, it increases the critical heat flux and then the needed flux in film boiling for a given temperature is also higher :

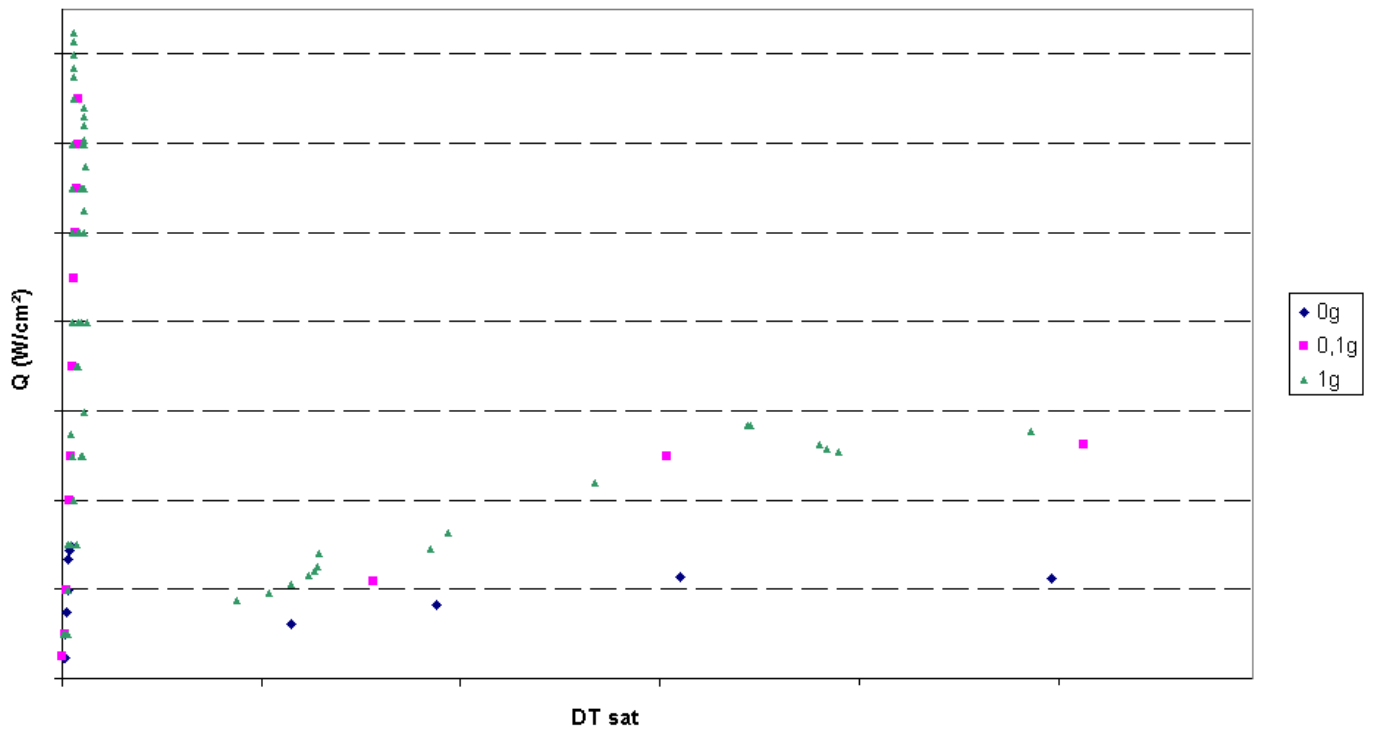


Figure 38: Comparison between different level of gravity for  $P=2$  bar and  $T=T_{sat} - 2k$

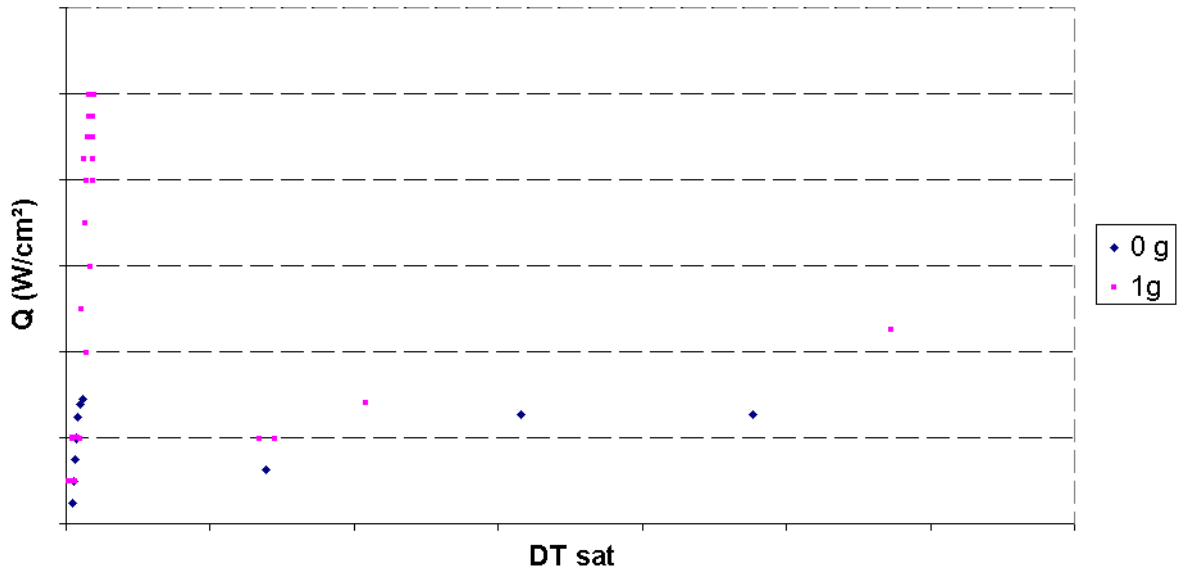


Figure 39: Comparison between different level of gravity for  $P=1$  bar and  $T=T_{sat} - 2k$

### 5.3.2 Effect of the pressure

Under the following conditions of gravity and temperature, when the pressure increases, the critical heat flux also increases. In the film region, the effect of the pressure seems to be more significant for small gravity.

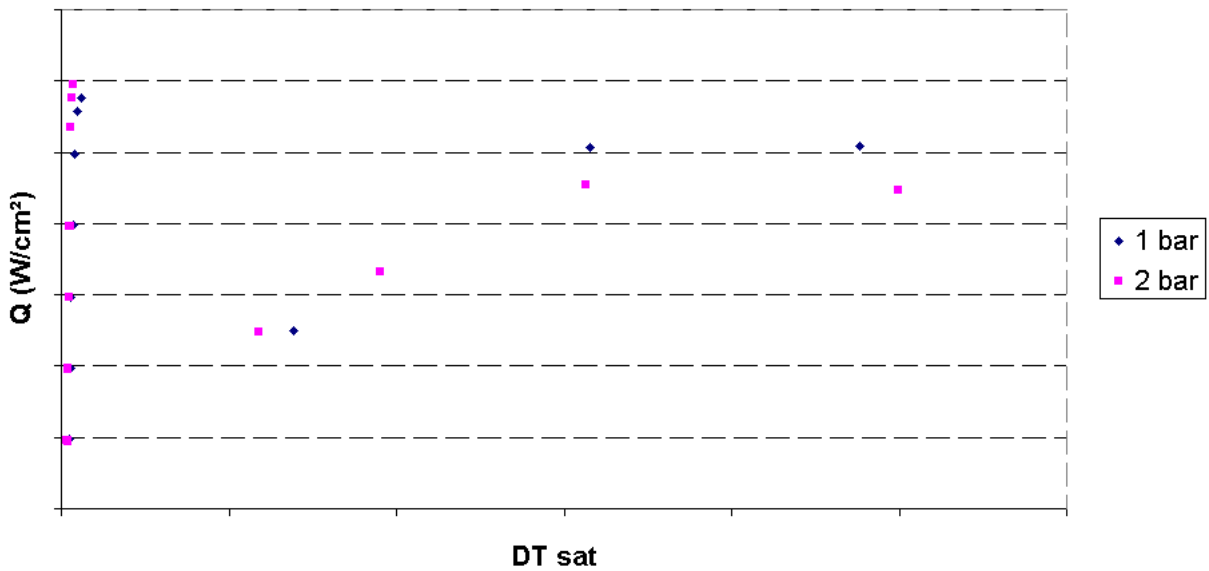


Figure 40: Comparison between the different pressure with the same level of gravity (0g) and subcooling :  $T=T_{sat} - 2K$

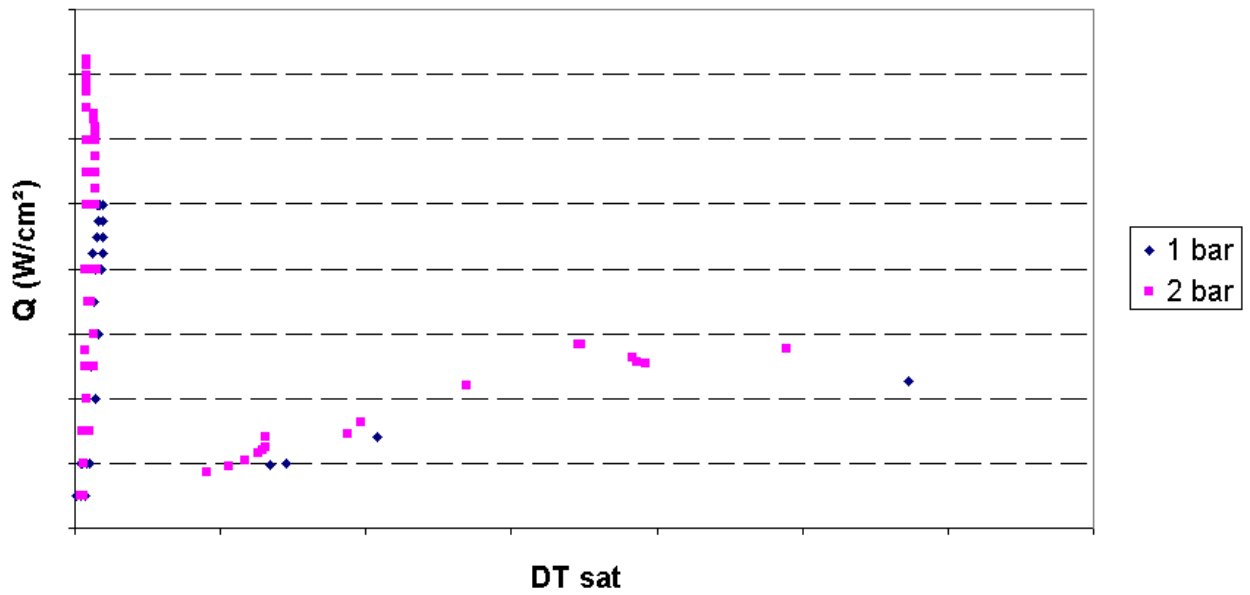


Figure 41: Comparison between the different pressure with the same level of gravity (1g) and subcooling :  $T = T_{sat} - 2K$

### 5.3.3 Effect of the subcooling

In the following condition of pressure and gravity, when the subcooling increases, the critical heat flux doesn't vary significantly.

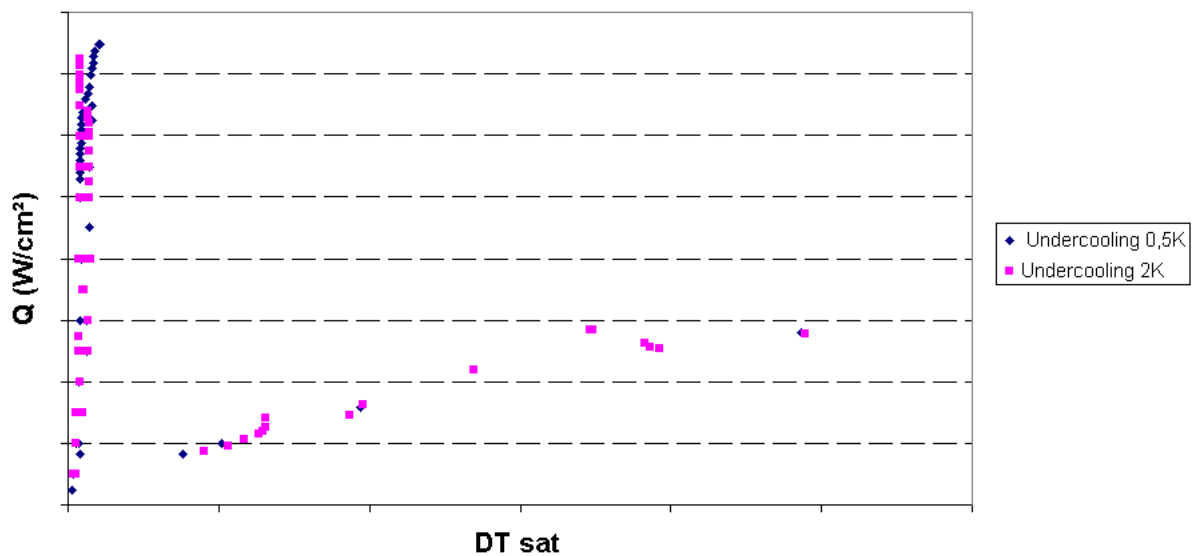


Figure 42: Comparison between the subcooling for the same pressure (2bar) and level of gravity (1g)

## 5.4 Problems encountered

In this section, some problems that have been encountered during experiment are presented.

### 5.4.1 Leakage in the cell feeding circuit

There is a small capillary in which the hydrogen gas goes through before entering the cell. Before this entrance to the cell, there are roughly 12 m of pipe until the hydrogen bottle: 2.5m inside the cryostat and the rest of it outside. There are three handling valves in this circuit which, in case of defects, can lead to pollute the incoming hydrogen.

It turned out that it happens for curve at 1g. That is probably the reason why these results are very dispersive: The liquid hydrogen was not the same between the beginning and the end of the experiment, since small amount of air (oxygen+ nitrogen) was slowly diluted in it.

Moreover, this leakage caused bigger problems: it plugged the capillary. Indeed, the solidification temperature of Oxygen is 60 K and the capillary was at 20K. It slowly created ice-plugs of oxygen. The speed of formation was certainly very slow due to the size of the leakage. Hence these ice-plugs were not present at the beginning of the experiment.

The major problem appeared at the end of the set of experiment, when the cell would have been emptied : while increasing the temperature, the liquid became gas. However, none of this gas could escape the cell, hence the pressure increased, following the phase diagram. The critical point for hydrogen is at 33K and the corresponding pressure is 13 bars. After this temperature, the fluid became supercritical. It was then impossible to exactly know what happened in the cell, even with the camera.

A video of the disappearance of the interface between normal fluid and supercritical fluid has been recorded, as it can be seen in figure 43.

Finally the ice-plugs melt and was ejected at 50–60K. Obviously, a huge peak of pressure has been measured while it happened. However, a security valve, regulated at 3 bar, evacuated the hydrogen before damaging anything.



Figure 43: Disappearance of the interface at the critical point

#### 5.4.2 Fast breakdown of the magnetic field

Because of the bad weather condition we had two brutal breakdowns of the current (and thus the magnetic field, going from 14T to 0T in 2s).

It created eddy currents in the copper exchangers of the cell and in the copper thermal shield all around. It resulted in a huge amount of energy (700 000 J), which instantaneously evaporated the whole cell (totally filled with liquid hydrogen). The pressure increased at such a point that the indium seal crept, letting the hydrogen gas going into the vacuum of the cryostat. Lorentz' force that resulted in this breakdown inflated the thermal shield and made it in its plastic stress. Then to remove this shield, an hydraulic jack has been used, as shown in the picture 44. 200 bars were applied to the piston, corresponding to a force of 14 300 N.



Figure 44: Use of an hydraulic jack to extract the thermal shield from the cryostat.

### 5.4.3 Losses in the cooling circuit

The previous problem damaged the shield. While a new one was made, the previous one was cut at the bottom and adapted to be able to continue experiments. An aluminium part was put to reduce radiation coming from the cryostat vacuum vessel (300K) as much as possible. However, It totally changed the behaviour of the cooling system, which was sized for the previous one.

The helium flow rate became insufficient to cool the cell. The understanding of what happened was no straightforward. The first idea has been to evaluate the losses in the gas siphon. This has been done by imposing a flow rate with a flowmeter placed directly at the output of the siphon. The temperature of the flow was measured. Hence, by using the formula:

$$\Phi = m' C_p (T_{out} - T_{in})$$

Where  $\Phi$  is the power,  $m'$  the flowrate and  $T_{in}$  and  $T_{out}$  the temperature at the entrance (in the helium tank, ie: 4.2K) and at the out of the siphon. Theses losses were estimated to 7 W, which gave a second explanation of the limitation in the cooling.

To be able to pursue our experiments, a pumping system has been installed at the output of the cooling (helium) system. Hence, the applied (relative) pressure in the pipes went from 0.5 bar to 1.5 bar, which enabled to increase the flowrate in the circuit and to continue cooling without any limitation.

## 6 Conclusion

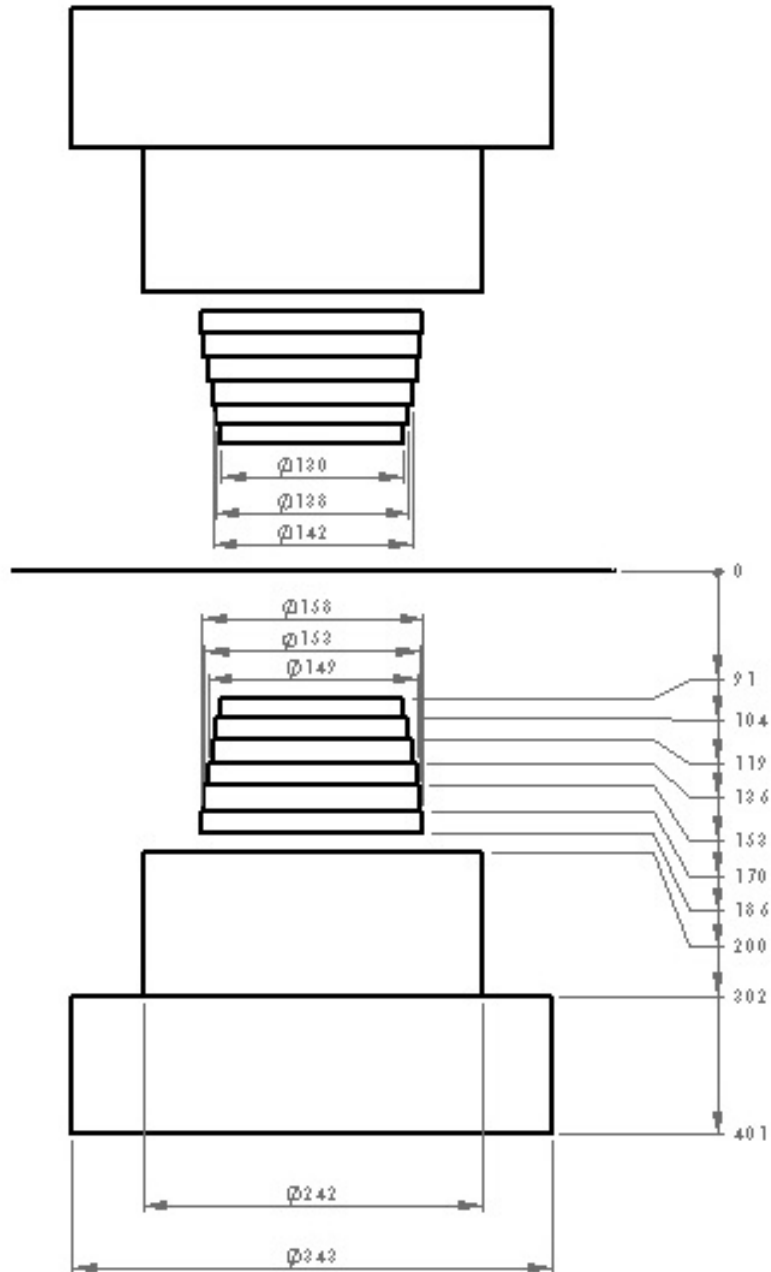
This master thesis enabled to have a good understanding of boiling heat transfers in microgravity. Different thermodynamic parameters have been studied independently one from each other to be able to draw solid conclusion regarding the behaviour of the fluid (liquid hydrogen) in such conditions. It also enabled to apply lots of different physics : mechanical behaviour at 20 K, cryogenics, vacuum technique, computational physics, magnetostatic behaviour, heat transfers...

It turns out that at 0g, the CHF is much lower than at 0.1 or 1g, whereas this CHF follows the increase of pressure.

Results are very satisfying and the main goal is achieved: This study can be used to design the new type of motor for Ariane spacecraft, that can be turned on into space after a while of inactivity.

# Appendices

## Drawing of the coil



Dimensions are given in mm

## List of Figures

1	Drop tower . . . . .	2
2	Airbus 0g . . . . .	3
3	Space shuttle . . . . .	4
4	Magnetic induction $B_z$ and Compensation $G_z$ on $z$ axe of the coil for Hydrogen . . . . .	8
5	Stability of magnetic compensation for diamagnetic fluids . . . . .	9
6	radial instability of an hydrogen bubble . . . . .	10
7	experimental devices : hot wire (on the left) and plat plate (on the right) $T_{sat}$ is the saturation temperature of the fluid . . . . .	14
8	Nukiyama curve . . . . .	14
9	Nucleate boiling. . . . .	15
10	Film boiling. . . . .	16
11	developement of a bubble . . . . .	17
12	Phase diagram of hydrogen . . . . .	20
13	Global drawing of the installation . . . . .	21
14	Moving of the cryostat with an overhead crane . . . . .	22
15	Inside of the cryostat (on the left) and top of the cryostat(on the right)	23
16	Observation system . . . . .	26
17	Modelisation of the cell (on the left) and real cell (on the right) . . . .	28
18	section of the bottom of the cell (on the left) and picture of the bottom of the real cell (on the right) . . . . .	29
19	Map of the residual gravity around half a cell . . . . .	31
20	Drawing of the principle element needed to size current supply wire. . .	32
21	Drawing of the principle elements in the vicinity of the thermal shield. .	34
22	Drawing of the thermal shield exchanger: the core (in orange) and the pipe (in blue). . . . .	36
23	Drawing of the fluid feeding system of the cell. . . . .	37
24	Time evolution of the heating element (TT100) during the detection of CHF . . . . .	41
25	Nukiyama's curve of liquid hydrogen at 1bar and the corresponding saturated temperature under 1g. . . . .	44
26	Nukiyama's curve of liquid hydrogen at 1bar and $T_{sat}$ -2K under 1g. . .	45
27	Nukiyama's curve of liquid hydrogen at 2bar and $T_{sat}$ -0.5K under 1g. . .	46
28	Nukiyama's curve of liquid hydrogen at 2bar and $T_{sat}$ -2K under 1g. . .	47
29	Nukiyama's curve of liquid hydrogen at 1bar and $T_{sat}$ -2K under 0g. . .	48
30	Snapshots of the video of nucleate boiling under 0g at 1bar and $T_{sat}$ -2K, from upper left corner to downner right one . . . . .	49
31	Snapshots of the video of nucleate boiling under 0g at 1bar and $T_{sat}$ -2K	49
32	Nukiyama's curve of liquid hydrogen at 2bar and $T_{sat}$ -2K under 0g. . .	50
33	Nukiyama's curve of liquid hydrogen at 2bar and $T_{sat}$ -2K under 0.1g. . .	51
34	Snapshots of the video of film boiling under 0.1g at 2bar and $T_{sat}$ -2K . .	51

35	Position of the thermal sensor in the heating compound (green rectangle on the top). . . . .	52
36	description of the different powers taking place in the heating compound.	53
37	Radial losses in the titanium ring . . . . .	55
38	Comparison between different level of gravity for P=2 bar and $T=T_{sat}-2k$	56
39	Comparison between different level of gravity for P=1 bar and $T=T_{sat}-2k$	57
40	Comparison between the different pressure with the same level of gravity (0g) and subcooling : $T=T_{sat}-2K$ . . . . .	57
41	Comparison between the different pressure with the same level of gravity (1g) and subcooling : $T=T_{sat}-2K$ . . . . .	58
42	Comparison between the subcooling for the same pressure (2bar) and level of gravity (1g) . . . . .	58
43	Disappearance of the interface at the critical point . . . . .	60
44	Use of an hydraulic jack to extract the thermal shield from the cryostat.	61

## List of Tables

1	Resume of the measurements that have to be performed . . . . .	43
2	Errors related to the measured power $P_{meas}$ . . . . .	54

## References

- [1] I.Rongier. Transport spatial en europe: enjeux et perspectives. Technical report, Journées CNES Jeunes Chercheurs, 2008.
- [2] *Boiling heat transfer for oxygen nitrogen and helium*. National Bureau of Standards, 1965.
- [3] A.Mailfert D.Chatain L.Quettier, H.Félice and D.Beysens. Magnetic compensation of gravity forces in liquid/gas mixtures: surpassing intrinsic limitations of a superconducting magnet by using ferromagnetic inserts. *the European Physical Journal Applied Physics*, 2005.
- [4] M.Lallemand. Transferts en changement de phase - ebullition libre. Technical report, Technique de l'ingénieur, 2005.
- [5] S.Nukiyama. The maximum and minimum values of the heat q transmitted from metal to boiling water under atmospheric pressure. *J.japan Soc. Mech*, 37:367–374, 1934.
- [6] Masahiro Shoji and Yuto Takagi. bubbling features from a single artificial cavity. *International Journal of Heat and Mass Ttransfer*, 2001.
- [7] C.Brennen. Fundamentals of multiphase flow. *Cambridge University Press*, 2005.